

RESEARCH ARTICLE

Inhibition of glial D-serine release rescues synaptic damage after brain injury

Stephen A. Tapanes¹  | Dena Arizanovska¹ | Madelen M. Díaz¹ |
Oluwarotimi O. Folorunso^{2,3} | Theresa Harvey³ | Stephanie E. Brown³ |
Inna Radzishevsky⁴ | Liesl N. Close¹ | Jonathan R. Jagid¹ |
Joacir Graciolli Cordeiro¹ | Herman Wolosker⁴ | Darrick T. Balu^{2,3} | Daniel J. Liebl¹ 

¹The Miami Project to Cure Paralysis, Department of Neurological Surgery, University of Miami Miller School of Medicine, Miami, Florida, USA

²Department of Psychiatry, Harvard Medical School, Boston, Massachusetts, USA

³Translational Psychiatry Laboratory, McLean Hospital, Belmont, Massachusetts, USA

⁴Department of Biochemistry, Rappaport Faculty of Medicine, Technion-Israel Institute of Technology, Haifa, Israel

Correspondence

Daniel J. Liebl, The Miami Project to Cure Paralysis, The University of Miami, 1095 NW 14th Terrace, R-48, Miami, FL 33136, USA.
Email: dliebl@miami.edu

Funding information

Allen and Jewell Prince Center for Neurodegenerative Disorders of the Brain; BrightFocus Foundation, Grant/Award Numbers: A20190345, 1R03AG063201-01; Israel Science Foundation, Grant/Award Number: 337/19; Lois Pope Life Foundation; Miami Project to Cure Paralysis, National Institute of Health/National Institute of Neurological Disorders and Stroke, Grant/Award Numbers: NS098740, NS120028, AG063201; US-Israel Binational Science Foundation, Grant/Award Number: 2019021

Abstract

Synaptic damage is one of the most prevalent pathophysiological responses to traumatic CNS injury and underlies much of the associated cognitive dysfunction; however, it is poorly understood. The D-amino acid, D-serine, serves as the primary co-agonist at synaptic NMDA receptors (NMDARs) and is a critical mediator of NMDAR-dependent transmission and synaptic plasticity. In physiological conditions, D-serine is produced and released by neurons from the enzymatic conversion of L-serine by serine racemase (SRR). However, under inflammatory conditions, glial cells become a major source of D-serine. Here, we report that D-serine synthesized by reactive glia plays a critical role in synaptic damage after traumatic brain injury (TBI) and identify the therapeutic potential of inhibiting glial D-serine release through the transporter Slc1a4 (ASCT1). Furthermore, using cell-specific genetic strategies and pharmacology, we demonstrate that TBI-induced synaptic damage and memory impairment requires D-serine synthesis and release from both reactive astrocytes and microglia. Analysis of the murine cortex and acutely resected human TBI brain also show increased SRR and Slc1a4 levels. Together, these findings support a novel role for glial D-serine in acute pathological dysfunction following brain trauma, whereby these reactive cells provide the excess co-agonist levels necessary to initiate NMDAR-mediated synaptic damage.

KEYWORDS

amino acid transporters, D-serine, neuroprotection, synaptic damage, traumatic brain injury

1 | INTRODUCTION

Traumatic brain injury (TBI) is a multifaceted pathological condition characterized by trauma to the head sufficient to disrupt homeostasis.

Worldwide, TBI affects nearly 69 million people annually and contributes to death and disability more than any other traumatic insult (Dewan et al., 2018; Prins et al., 2013; Taylor et al., 2017). Injury severity can range from mild concussion to severe trauma, with many TBI patients suffering from acute and/or chronic cognitive dysfunction (McGinn & Povlishock, 2016; Prins et al., 2013). Disruption of the neuronal circuitry

Stephen A. Tapanes and Dena Arizanovska co-contributing authors.

This is an open access article under the terms of the Creative Commons Attribution-NonCommercial License, which permits use, distribution and reproduction in any medium, provided the original work is properly cited and is not used for commercial purposes.

© 2022 The Authors. GLIA published by Wiley Periodicals LLC.

is one underlying pathology associated with cognitive dysfunction, where damage to the hippocampal circuitry leads to learning and memory deficits (Perez et al., 2017). The hippocampal tripartite synapse consists of an integration of pre- and post-synaptic neuronal membranes with glial cells that actively facilitates synaptic plasticity and transmission (Eroglu & Barres, 2010; Perea et al., 2009). The widespread gliotic response of astrocytes and microglia are well characterized in the injured brain (Adams & Gallo, 2018; Bradbury & Burnside, 2019; Wang et al., 2018); however, the effects of gliosis on the tripartite synapse remain largely unexplored.

NMDA receptors (NMDARs) play critical roles in regulating synaptic transmission and plasticity, but also have been implicated in glutamate-induced excitotoxic cell death (Faden et al., 1989; McGinn & Povlishock, 2016; Prins et al., 2013). More recently, hyperactivation of NMDARs by the co-agonist D-serine after TBI is thought to lead to hippocampal synaptic damage in the absence of cell death, suggesting that D-serine plays a critical role in regulating synaptic stability (Billard, 2012; Perez et al., 2017; Wolosker, 2018). In physiological conditions, D-serine is a product of enzymatic L-serine conversion by serine racemase (SRR), which is released postsynaptically (Wong et al., 2020) by neurons to modulate NMDAR activity (Martineau et al., 2014; Shleper et al., 2005; Wolosker, 2011; Wolosker et al., 2016). In a murine controlled cortical impact (CCI) injury model, we have shown that pathological increases in SRR and D-serine synthesis in reactive astrocytes contribute to deficits in synaptic plasticity and memory (Perez et al., 2017). However, whether reactive microglia also produce D-serine and the mechanism(s) by which reactive glia release D-serine after TBI is unknown. D-serine release can occur by vesicular (Mothet et al., 2005) and transport mechanisms (Bodner et al., 2020; Ehmsen et al., 2016; Fukasawa et al., 2000; Jeon et al., 2009; Rosenberg et al., 2013; Sakai et al., 2003); however, two amino acid transporters have been strongly implicated in both the influx and efflux of D-serine, namely, Slc1a4 (ASCT1) and Slc7a10 (asc-1) (Foster et al., 2016; Kaplan et al., 2018; Neame et al., 2019; Sason et al., 2017). Slc7a10 is also present to a lesser extent in neurons (Helboe et al., 2003; Safory et al., 2015). Because D-serine levels in the extracellular synaptic space are important in NMDAR activation and learning and memory (Foster et al., 2016, 2017; Kaplan et al., 2018; Rosenberg et al., 2013; Sason et al., 2017), it is important to understand the role of these transporters in pathological conditions. Specifically, as NMDARs can have both neuroprotective and neurotoxic effects after injury (Bading, 2017; Ikonomidou & Turski, 2002), targeting glial D-serine transporters may provide a novel avenue to modulate hyperactivation of NMDARs without altering all glutamatergic signaling.

Here, we utilize pharmacological and genetic approaches to show that injury-induced microgliosis and astrogliosis mediate synaptic damage after TBI through enhanced D-serine synthesis by SRR and release by the Slc1a4 transporter. Increases in SRR and Slc1a4 levels are also observed in tissues resected from human TBI patients, thus supporting the therapeutic relevance of our D-serine mediated model of synaptic damage.

2 | MATERIALS AND METHODS

2.1 | Study design

Genetically modified male mice were randomly assigned to a CCI or sham control surgery and evaluated for synaptic losses and cognitive dysfunction at multiple predetermined endpoints (3, 7, and 28 dpi). The primary techniques used include: Golgi analysis, IHC, flow cytometry, quantitative reverse transcription polymerase chain reaction (qRT-PCR), and fear conditioning. Animal numbers were calculated by power analysis with the G*Power 3.1 calculator based on the effect size in our preliminary experiments, when possible. Given our experimental design, we used the Multiple ANOVA-Global effects test with effect size ranging from 0.2 to 0.8, power = 0.8; and $\alpha = .05$. Treatment and control groups consisted of littermates and were evaluated together whenever possible, based on the numbers of animals born in the facilities. Confounders such as order of surgery and/or treatment, cage location in facilities, and experimental design based on the calendar year were not controlled. Experimenters were blinded to the animal genotype and condition during behavioral testing, tissue collection, and data analysis. No animals were excluded from study, and experiments were run in technical triplicate.

2.2 | Animals

All procedures related to animal use and care were approved by the University of Miami Animal Use and Care Committee (protocol #20-061). Male adult C57BL/6 mice ages 2–4 months were used for all experiments. Experimental $SRR^{fl/fl}$ and $Slc1a4^{fl/fl}$ mice were generated by crossing mice to cell-specific cre expressing mice, including astrocytic $hGFAP^{CreERT2}$ (Jackson Laboratory, Bar Harbor, ME; B6.Cg-Tg(GFAP-cre/ERT2)505Fmv/J), microglial $CX_3CR_1^{CreERT2}$ (Jackson Laboratory; B6.129P2(Cg)-Cx3cr1^{tm2.1(cre/ERT2)Litt}/WganJ), and microglial $TMEM119^{CreERT2}$ (Jackson Laboratory; C57BL/6-Tmem119^{em2(EGFP)Gfng}/J) mice. Germline deficient $SRR^{-/-}$ mice were previously reported (Benneyworth et al., 2012). $Slc1a4^{tm1a(KOMP)Wtsi}$ mice (UC Davis KOMP center) contain loxP sites flanking exon 4, and a lacZ-Neo cassette is localized to the intron between exons 3 and 4. Mice carrying the LacZ reporter gene driven by the $Slc1a4$ promoter, were referred to as $Slc1a4^{LacZ}$ and were only used for expression studies. Flp excision of lacZ-Neo cassette resulted from mating $Slc1a4^{tm1a(KOMP)Wtsi}$ mice with $B6.Cg-Tg^{(Pdgk1-flpo)105ykr/J}$ mice (Jackson Laboratory) to produce the $Slc1a4^{fl/fl}$ mouse line.

Cre recombinase was induced between 2–4 weeks prior to experimentation by intraperitoneal (i.p.) injections of 90 mg/kg Tamoxifen (TAM; MilliporeSigma, St. Louis, MO) for 1 day, followed by 2 days of rest, followed by 5 consecutive days of injections. TAM was dissolved in a vehicle of 90% sunflower oil and 10% ethanol. All animals received TAM treatment at least 2 weeks prior to any experimental procedure unless otherwise stated, including control $SRR^{fl/fl}$ and $Slc1a4^{fl/fl}$ mice without Cre-recombinase. All mice were group-housed under a 12/12 h light/dark cycle and had access to food and water *ad libitum*.

2.3 | Controlled cortical impact injury

Mice were anesthetized with a ketamine-xylazine cocktail (100/10 mg/kg, respectively) and maintained on a heating pad for the duration of the procedure. A skin incision was made to expose the skull and then the head was placed in a stereotaxic frame for CCI. Following a 5 mm craniotomy, a 3 mm pneumatic piston was used to produce the CCI injury over the right parieto-temporal cortex at a velocity of 4 m/s, depth of 0.55 mm, and duration of 150 ms using an eCCI-6.0 device (Custom Design & Fabrication, Brookings, SD). Coordinates of the injury epicenter were: -2.0 mm from bregma, lateral 2.5 mm. Following CCI injury, the skin was closed using 5-0 Vicryl synthetic nylon sutures and mice were placed on a heating pad, injected with 1 mL of lactated Ringer's solution, slow-release buprenorphine (1 mg/kg), and monitored twice daily for 1-week postinjury.

2.4 | D-serine immunohistochemistry

Mice were intracardially perfused with a fixative of 3% glutaraldehyde (#111-30-8, Electron Microscopy Sciences, Hatfield, PA), 1% paraformaldehyde (PFA, #76240, MilliporeSigma), 0.2% sodium metabisulfite (MilliporeSigma) and 10 U/mL Heparin salt (MilliporeSigma). Brains were postfixed in fixative for 24 h and cryoprotected in 30% sucrose. D-serine IHC was performed on 20 μ m free-floating sections as previously described (Balu et al., 2014). Briefly, sections were incubated with 0.5% NaBH₄ and 0.2% sodium metabisulfite in TBS (pH 7.4) for 10 min. Endogenous peroxidases were quenched by incubating sections with 0.3% H₂O₂ in TBS (pH 7.4) for 30 min. Sections were blocked with 10% normal goat serum and 0.1% triton X-100 in TBS for 1 h at RT. Rabbit α D-serine antibody (1:1000, #6472, Abcam, Waltham, MA) was diluted in a blocking solution containing 5 mM L-serine-glutaraldehyde-BSA conjugate and sections incubated for ~40 h at 4°C. Sections were incubated with Goat α Rb IMPRESS HRP reagent (#MP7451, Vector, Burlingame, CA) for 60 min at RT followed by incubation with IMMPACT DAB (#SK4105, Vector) for appx 7 min. All tissue sections were treated in parallel and in a blinded manner. Images were collected on a Zeiss Axioskop microscope using StereoInvestigator software (MBF Bioscience; Welliston, VT).

2.5 | Immunofluorescence

Mice were intracardially perfused with 1x PBS (pH 7.4) followed by 4% PFA (MilliporeSigma) in 1x PBS. Brains were postfixed in 4% PFA for 24 h, cryoprotected for 24 h in 30% sucrose and sectioned at 30 μ m. Sections were incubated with 3% H₂O₂ in 1X PBS for 20 min followed by three 1xPBS washes. For SRR IHC, sections were blocked with 10% Donkey serum, 1% BSA, 0.1% Triton-100 in 1X PBS for 1 h at RT. To block endogenous Mouse IgG, sections were incubated with Unconjugated AffiniPure Fab Fragment Goat α Mouse IgG (H+L) (1:10; #715-007-003, Jackson Immuno, West Grove, PA) for 2 h at

RT. Sections were then incubated with primary Ab overnight at 4°C (mouse α SRR (BD Biosciences, #312053, 1:150; rabbit α GFAP, #7260, 1:1000; goat α ba1, #NB100-1020, 1:400). Sections were incubated with secondary antibodies (Donkey α Mouse Fab Alexa 647 1:500, Donkey α Goat Alexa 568, Donkey α Rabbit Alexa 488, 1:500) for 1 h at RT. Sections were then washed three times with 1X PBS for 5 min each. For nuclei staining, sections were incubated in Hoechst 33342 (1:5000; #3750, ThermoFisher, Waltham, MA).

2.6 | β -gal staining and antibody co-labeling

LacZ tissues were prepared similar to IHC with the exception of no overnight postfixation in 4% PFA. Sections were washed with 0.1M PB (pH 7.4), rinsed 3 \times 15 min, and treated with β -galactosidase (β -gal) staining solution for 6 h at 37°C, washed with PB, dehydrated, and coverslipped. The rinse solution was composed of 0.02% IGEAL CA-650 (MilliporeSigma), 0.01% sodium deoxycholate (MilliporeSigma), 1.25 mM EDTA (MilliporeSigma), and 2 mM MgCl₂ (MilliporeSigma) in 0.1M PB. The stain solution contains 1 mg/mL X-gal (#X4281C, Goldbio, St. Louis, MO) and 0.4 mg/mL nitroblue tetrazolium (NBT; #11383213001 MilliporeSigma) in rinse solution. Co-labeling was performed with α GFAP and α ba-1 prior to β -gal staining and imaged on a Leica TCS SP5 confocal microscope at 10 \times magnification. Coverslips were then removed and sections were treated as described above for β -gal staining.

2.7 | Human TBI patient tissues and analysis

The collection of human TBI brain tissues was approved by the University of Miami Institutional Review Board (protocol #20080609), and written informed consent was obtained for each patient according to the Declaration of Helsinki. During surgery an average of 100–1000 mg of tissue is removed from the perilesional injury site using a pituitary rongeur prior to suction debridement. Samples were immediately placed in a sterile container and kept on ice until transfer to a -80°C freezer for storage. Control cortical protein lysates (#NB820-59186, NB820-60574, NB820-59193, NB820-59198, and NB820-59177, Novus Biologicals, Centennial, CO; #P3234073 and P3234051, BioChain, San Francisco, CA) and RNA samples (#636570, 636571, and 636564, Takara Bio, Kusatsu, Japan) were obtained from cardiac arrest cases without known co-morbidities. A total of 12 patient samples without known CNS co-morbidities were evaluated (see Table 1).

2.8 | Western blot

Hippocampi of ipsilateral sham or CCI injured wild-type mice were lysed in RIPA buffer with protease (#04693159001, MilliporeSigma) and phosphatase inhibitors (#04906845001, MilliporeSigma). Samples were incubated for 20 min on ice and centrifuged at 4°C (13.2 rpm, 10 min).

TABLE 1 Injury and demographic information on human brain samples

Sample ID	Reason	Region	GCS at arrival	Time (days from arrival to surgery)	Age	Sex	Race
C1 (protein)	Cardiac arrest	WB	N/A	N/A	82	M	N/A
C2 (protein)	Cardiac arrest	CC	N/A	N/A	22	M	N/A
C3 (protein)	Cardiac arrest	F	N/A	N/A	22	M	N/A
C4 (protein)	Cardiac arrest	T	N/A	N/A	66	M	N/A
C5 (protein)	Cardiac arrest	F	N/A	N/A	82	M	N/A
C6 (protein)	Cardiac arrest	T	N/A	N/A	77	M	N/A
C7 (protein)	Cardiac arrest	P	N/A	N/A	66	M	N/A
C8 (RNA)	Cardiac arrest	O	N/A	N/A	22–68	14 M/Fe	W
C9 (RNA)	Cardiac arrest	P	N/A	N/A	35–89	4 M/Fe	W
C10 (RNA)	Cardiac arrest	T	N/A	N/A	21–82	5 M	A
IDO	Fall	F	10	8	32	M	W
CLR	GSW	P/O	14	2	21	M	B
AP	MVA	F	7T	6	50	M	W
IVG	MVA	T	13, rapidly deteriorating	≤1	76	M	B
MC	Fall	F	7T	2	54	F	B
MM	GSW	T	7T	≤1	18	M	B
RRP	MVA	F	10	≤1	63	M	W
PD	Fall	T	6T	≤1	28	F	W
NA	Bike accident	T	7	≤1	44	M	H
JCVH	MVA	T	7T	4	34	M	H
JSTL	MVA	T	3	≤1	58	M	N/A
JB	MVA	T	3	≤1	29	M	H

Note: A total of 12 TBI patients were processed for Western blot and qPCR analysis. C1–C10 reference control samples, where a score of 1–8 is classified as a severe injury, 9–12 as moderate, and 13–15 as mild; T indicates the patient is intubated.

Abbreviations: a, asian; B, black; CC, cerebral cortex; Fe, female; F, frontal; GCS, glasgow coma scale; GSW, gunshot wound; H, hispanic; M, male; MVA, motor vehicle accident; O, occipital; P, parietal; T, temporal; W, white; WB, whole brain.

The supernatant was further processed using the Quick Start Bovine Serum Albumin (BSA) Standard kit (#5000206, Bio-Rad, Hercules, CA) to determine protein concentration. Human samples were incubated overnight at 37°C with the Protein Deglycosylation Mix II (#P6044S, New England BioLabs, Ipswich, MA) according to the manufacturer's instructions. Samples were diluted to 30 µg and separated on a 4%–20% gradient gel (#5678095, Bio-Rad), followed by transfer to a nitrocellulose membrane using the Trans-Blot Turbo RTA Transfer Kit (#1704270, Bio-Rad). Membranes were incubated with 5% BSA in PBS for 1 h at RT followed by overnight incubation at 4°C with primary antibodies: αSRR (1:1000, #sc-365217, Santa Cruz Biotechnology, Dallas, TX), αSlc1a4 (1:1000, #8442S, Cell Signaling, Danvers, MA) and αGAPDH (1:5000, #sc-47724, Santa Cruz Biotechnology). Membranes were washed three times for 15 min in 1X TBS with 0.1% Tween-20 and incubated for 2 h at RT with secondary antibodies diluted 1:5000: goat α-rabbit (#111-035-003, Jackson Immuno) and goat α-mouse (#115-035-071, Jackson Immuno). Membranes were exposed using the SuperSignal West Pico PLUS Chemiluminescent Substrate (#34578, ThermoFisher) substrate and visualized using the ChemiDoc Touch Imaging System (Version 1.2.0.12, Bio-Rad). Densitometry analysis was performed using the Image Lab software (Bio-Rad), where protein measurements were

normalized to GAPDH for human samples and total protein for mouse samples. A whole brain control sample was used to standardize between gels; measurements were then normalized to average cortical control values.

2.9 | RNA extraction and qRT-PCR

RNA was extracted from the ipsilateral hippocampi of sham or CCI injured wild-type mice with the Direct-zol RNA miniprep kit according to the manufacturer's instructions (#R2051, Zymo Research, Irvine, CA). RNA concentration and quality was determined with the NanoDrop 1000 Spectrophotometer (ThermoFisher). Only RNA with a 260/280 ratio of >2.0 was used. 400–500 ng of input RNA was reverse transcribed into cDNA using a High-Capacity cDNA reverse transcription kit (#4368814, ThermoFisher) for qRT-PCR. For fluorescence-activated cell sorting (FACS) isolated cells, used the PicoPure RNA isolation kit (#KIT0214, ThermoFisher) for RNA extraction, and genes of interest were preamplified for 13 cycles. qPCR was performed using AmpliTaq Gold 360 Master Mix (#4398881, ThermoFisher) with 50 nM ROX passive reference dye (#75768,

ThermoFisher), a QuantStudio 3 Thermocycler (ThermoFisher), and TaqMan primers (*SRR*, Hs00926869_m1; *SLC1A4* Hs00161719_m1; *Slc1a4*, Mm01223875_m1; *Slc1a5*, Mm00436603_m1; *Slc7a10*, Mm00502045_m1; and *Daa0* Mm00438378_m1, ThermoFisher). Glyceraldehyde 3-phosphate dehydrogenase (*Gapdh*, Mm99999915_g1 and Hs02786624_g1, ThermoFisher) was used as an endogenous control. ΔCt was calculated by subtracting the *GAPDH* Ct from its respective sample's target gene(s) Ct, and $\Delta\Delta\text{Ct}$ was calculated by subtracting the average ΔCt of reference samples from the ΔCt of experimental samples. The absence of reverse transcriptase (i.e., no RT) was used as a negative control. Fold difference is equal to $2^{-\Delta\Delta\text{Ct}}$. Data were presented as Log_2 of the Fold Difference. Samples were run in duplicate or triplicate. All analyses were performed in a randomized nonbiased manner.

2.10 | Golgi staining and analysis

Mice were anesthetized and whole brains immediately harvested. Following the Rapid Golgi Kit manufacturer's protocol (#PK401, FD Neurotech, Columbia, MD), brains were placed in a 1:1 mixture of solutions A and B for 2 weeks followed by solution C for 72 h. Brains were then snap frozen on dry ice, cryosectioned at 120 μm (Leica CM1850), and collected onto gelatin coated slides. Samples were stained following the manufacturer's protocol. Briefly, sections were washed with water and submerged in a staining solution composed of solution D, solution E, and water for 10 min. Samples were then rinsed in water, progressively dehydrated in ethanol, and treated with xylene prior to cover-slipping with Permount mounting medium (#SP14-100, ThermoFisher). Sections were imaged on an Olympus IX70 microscope with a 100 \times objective and 1.5 \times zoom for a working magnification of 150 \times . Three dendritic segments (>10 μm in length) in the *stratum radiatum* were imaged per cell, where three separate cells were analyzed per animal for a total of nine segments per animal from primary branches of the apical dendrite. 0.2 μm Z-stack optical sections were used while imaging to generate z-stacks. Image analysis was done as previously described (Risher et al., 2014). Briefly, image stacks were imported into Reconstruct software (Harris Lab, Center for Learning and Memory, University of Texas, Austin, TX) to analyze Z-length, dendritic spine number, and dendritic spine morphology. Morphology was characterized based on length and width, where a width >0.6 μm denoted a mushroom spine and a length > 1 μm denoted a thin spine. All analyses were performed in a randomized nonbiased manner and experimenters were blinded to condition and genotype.

2.11 | Fluorescence-activated cell sorting

Mice were transcardially perfused with PBS and CCI injured ipsilateral hippocampi were harvested. No fixative was used during perfusion for FACS isolation. Tissue was dissociated into single cells with an adult brain dissociation kit (#130-107-677, Miltenyi Biotech, Bergisch Gladbach, Germany) and gentleMACS dissociator (#130-093-235,

Miltenyi Biotech) according to a modified manufacturer's protocol. For HPLC, the procedure was modified to include 250 μM L-4-Chlorophenylglycine (L4) and 5 μM BMS-466442 (BMS) to all isolation solutions/steps to minimize D-serine release. To measure cell viability, single cell suspensions were incubated for 1 h at 4°C with Ghost Violet 540 viability dye (#13-0879-T100, Tonbo Biosciences, San Diego, CA). Cells were then labeled with $\alpha\text{CSA-2}$ (1:50; #130-116-141, Miltenyi Biotech), αCD11b (1:50; #130-113-802, Miltenyi Biotech), and αCD45 (1:100; #103114, Biolegend, San Diego, CA) for 30 min at 4°C. Samples were sorted on a MoFlo Astrios Cell Sorter (Beckman Coulter, Brea, CA) into PBS for HPLC, centrifuged (5000 $\times g$ for 10 min), resuspended in 6% Trichloroacetic acid, and frozen at -80°C and shipped on dry ice for HPLC analysis.

2.12 | High-performance liquid chromatography

FACS-isolated cells were immediately lysed with 6% trichloroacetic acid and cleared by centrifugation (16,000 $\times g$ for 10 min). The supernatant was extracted five times with water-saturated ether to remove TCA and diluted into 20 mM borate buffer at pH 9.0. The samples were derivatized for 50 s with *N-tert*-butyloxycarbonyl-L-cysteine and *o*-phthalaldehyde (MilliporeSigma), using 100 pmol L-2-aminoadipic acid (MilliporeSigma) as internal standard. Samples were separated using two coupled Chromolith RP-18 endcapped 100-4.6 HPLC columns (Merck, Kenilworth, NJ) in a Hitachi HPLC apparatus (Tokyo, Japan) consisting of a pump (L-7100), autosampler (L-7250), fluorescent detector (L-7485), and degasser (L-7614). To monitor D-serine and other amino acids, we acquired ~120,000 microglial cells and ~45,000 astrocytes ($n = 4$ combined hippocampi per run per group) for HPLC. For the analysis of endogenous D-serine in the hippocampus, the tissues were weighed and treated with 20 volumes of TCA 6% and processed as described above.

2.13 | Flow cytometry

For flow cytometry experiments, samples underwent treatment similar to FACS samples with the exception of intracellular and DAPI staining to improve separation. Following cell-surface labeling, samples were fixed with 1% PFA and 0.5% Tween-20 in PBS for 1 h at RT. Samples were centrifuged, resuspended in 100 μL of flow buffer, and blocked with an FcR blocking reagent (#130-092-575, Miltenyi Biotech) or a mouse αSRR antibody (1:1000, #612053, BD Biosciences) for 1 h at RT followed by staining with a goat α -mouse-488 nm secondary antibody (#A1101, ThermoFisher) for 30 min at RT. Samples were then centrifuged, resuspended in 250 μL flow buffer, treated with 1 drop of NucBlue Fixed Cell DAPI (#R37606, ThermoFisher) and analyzed with a Cytoflex S flow cytometer (Beckman Coulter) and analyzed with CytExpert (Beckman Coulter) software. Gating was set based on fluorescent signal from unstained and single channel control samples: astrocytes were positive for *CSA-2* expression, whereas microglia expressed high levels of CD11b and low levels of CD45 (to distinguish from CD45^{high}



macrophages) (Figure S2). Flow buffer consisted of PBS with 0.5% BSA and 2 mM EDTA, pH 7.2.

2.14 | Fear conditioning

At 5- or 26-days postinjury (dpi), mice were placed in a fear-conditioning apparatus (30 × 24 × 21 cm (Coulbourn Instruments, Allentown, PA)) with an electric grid floor (0.8-cm spacing, 4.8-mm diameter rods) for habituation for 600 s. Twenty-four hours after habituation (6 or 27 dpi), mice were placed back in the apparatus for a total of 210 s; at 120 s, mice were exposed to a 30-s tone (85 dB, 2 kHz) followed by a 0.7-mA foot shock for the last 2 s of the tone. Twenty-four hours after training (7 or 28 dpi), mice were returned to the apparatus and freezing behavior was measured for 300 s to assess contextual fear conditioning. The box was cleaned with 70% EtOH and an enzymatic cleaner between animals. Freezing behavior was quantified with video-based analysis software (FreezeFrame 3, Coulbourn Instruments).

2.15 | Small molecules

L-4-Chlorophenylglycine (L4), a selective Slc1a4 inhibitor (CAS 67336-19-0; #103114, Santa Cruz Biotechnology, Dallas, TX) (Foster et al., 2017), was dissolved in NaOH and diluted in PBS to a stock concentration of 2.5 mM (10X; pH 7.4). BMS-466442 (BMS), a selective noncompetitive Slc7a10 inhibitor, was obtained from Dr. Herman Wolosker (Brown et al., 2014). BMS was dissolved in 100% DMSO at 5 mM (1000X working stock). Both compounds were provided at pharmaceutical grade of >98% pure. L4 and BMS stock solutions were diluted in PBS to their final working concentrations of 250 and 5 μM, respectively.

Alzet pumps (#0000290, 0000296, Alzet, Cupertino, CA) were preloaded to deliver 5 μM BMS, 250 μM L4, or vehicle (PBS) for 7 or 14 days after implantation. Loaded pumps were connected to a brain infusion catheter (#0008851, Alzet) and placed in 0.9% saline at 37°C overnight to equilibrate. Immediately after CCI, the infusion device was lowered using a stereotactic holder until the tip of the cannula reached the lateral ventricle (−2.0 mm from dura). The cannula was secured to the skull without disturbing the injury using Loctite 454 Prism Gel (#233998, Henkel Corp., Bridgewater, NJ). The Alzet pump was placed in a subcutaneous pocket in the back of the neck and the incision of the skull sutured. Mice were housed separately in clean heated cages and allowed to recover.

2.16 | Statistics

Data was analyzed with Student's two-tailed *t*-test or 1-way or 2-way ANOVA with Tukey's multiple comparisons using GraphPad Prism 7. Prior to analysis, data was analyzed for normality and homoscedasticity. *, **, and *** represent *p*-values of .05, .01, and .001, respectively, within groups. #, ##, and ### represent *p*-values of .05, .01,

and .001, respectively, as compared with sham counterparts. Data is presented as mean ± SEM. All analyses were performed in a randomized nonbiased manner.

3 | RESULTS

3.1 | Increased serine racemase expression in reactive microglia and astrocytes after CCI injury

In nonpathological conditions, SRR expression is primarily restricted to the excitatory pyramidal cell (*pyr*) layer and dentate granule cell (*dgc*) layer, as well as dendrites, in the adult mouse hippocampus (Figure 1a), supporting previous observations (Balu et al., 2014; Benneyworth et al., 2012; Perez et al., 2017; Wong et al., 2020). Astrocytes and microglial cells are uniformly distributed throughout the hippocampus as observed by the astrocytic glial fibrillary acidic protein (GFAP) marker (Figure 1b) and the microglial ionized calcium binding adaptor molecule 1 (*Iba-1*) marker (Figure 1c). In these non-pathological sham tissues, we observe basal GFAP and *Iba-1* expression levels that are associated with little to no glial SRR expression. Moderate–severe murine CCI injury results in severe cortical tissue damage with moderate damage to the hippocampus as previously shown (Perez et al., 2016). In particular, we observed glial activation and synaptic damage in the hippocampus without the loss of neurons in the *pyr* or *dgc* layers (Perez et al., 2016). At 3 days post-CCI injury (dpi), SRR expression is no longer restricted to the *pyr* and *dgc* layers, but instead observed uniformly throughout the hippocampus (Figure 1d). Hippocampal SRR expression corresponded with increased astrocytic (Figure 1e) and microglial (Figure 1f) activation, where we observed increases in GFAP and *Iba-1* expression, as well as morphological alterations. High-magnification images of the sham and CCI injured tissues show SRR localization (white) in both astrocytes (Figure 1g–j) and microglia (Figure 1k–n) at 3 and 7 dpi. To validate our immunofluorescent observations of glial SRR expression, we examined SRR localization following CCI injury using cell-type specific SRR knockout mice. We bred transgenic mice that have the first coding exon of *Srr* flanked by loxP sites, with mice that express a tamoxifen inducible Cre recombinase either in microglia ($CX_3CR_1^{creErt2};SRR^{fl/fl}$ mice) or astrocytes ($GFAP^{creErt2};SRR^{fl/fl}$ mice). Figure S1 shows that after CCI injury, $GFAP^{creErt2};SRR^{fl/fl}$ mice retained SRR expression in microglia and $CX_3CR_1^{creErt2};SRR^{fl/fl}$ mice retained SRR expression in astrocytes, thus validating our cell-type specific strategy.

To provide a secondary measure of expression, we used flow cytometry to evaluate the percent of microglia and astrocytes expressing SRR (Figure 1o) as well as the mean SRR fluorescent intensity per cell (Figure 1p). Microglia were identified as viable CD11b⁺/CD45^{low}-labeled cells and astrocytes as viable CD11b[−]/CD45[−]/ACSA-2⁺ (astrocyte cell-surface antigen 2)-labeled cells. Cell-type purities were validated by quantifying *CD11b* and *GFAP* mRNA expression levels (Figure S2). Microglial cells showed a significant 30%–35% increase in the percent of SRR expressing cells at 3 and 7 dpi, in addition to a 2.0- to 2.5-fold increase in mean SRR

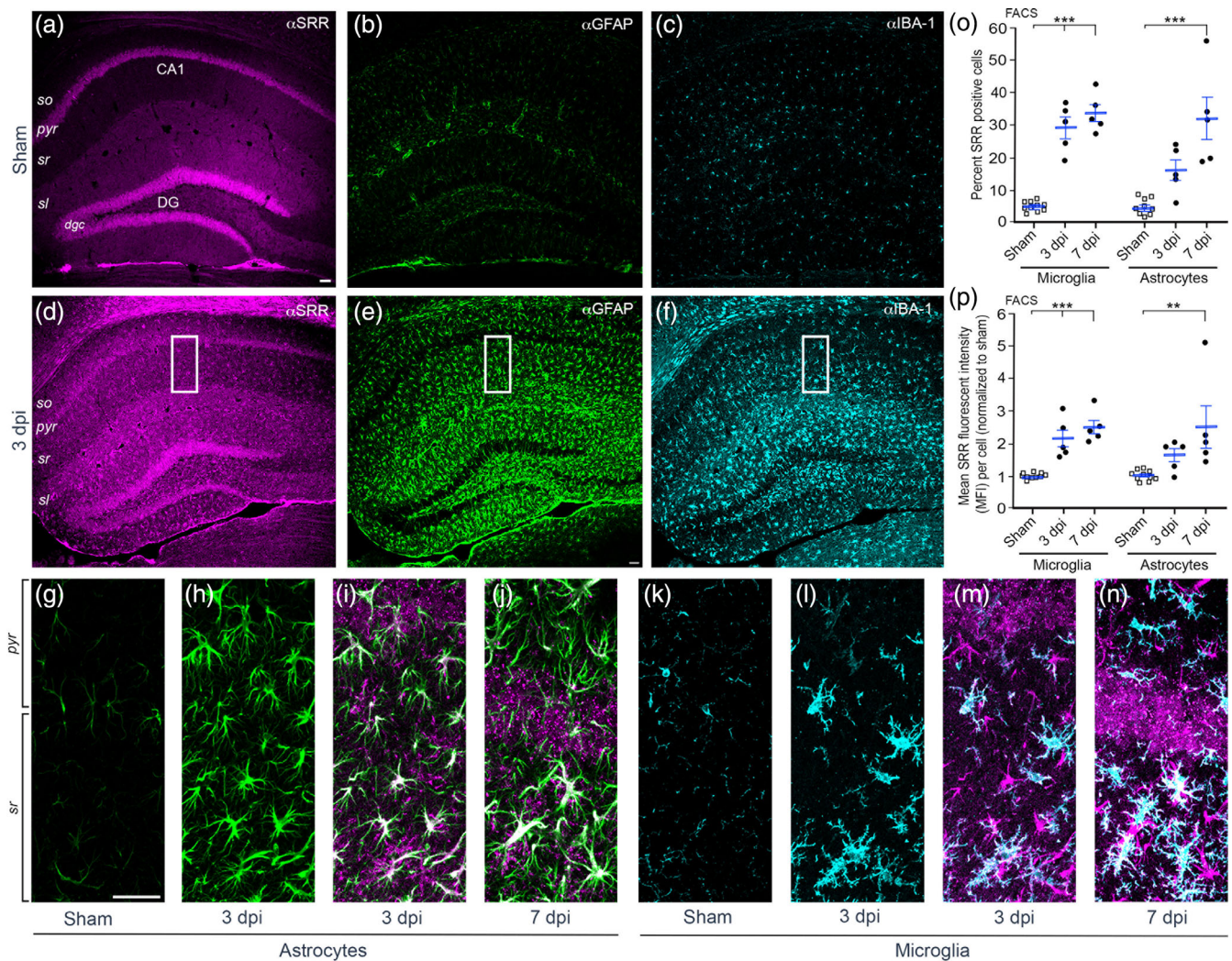


FIGURE 1 Serine racemase (SRR) is expressed by hippocampal microglia and astrocytes following CCI injury. (a) SRR is primarily expressed in the soma and dendrites of hippocampal pyramidal and dentate granule neurons. Under sham conditions there is very little gliosis in the sham hippocampus as measured by α GFAP (b) and α IBA-1 (c) immunofluorescence expression. At 3 dpi, SRR expression (d) is reduced in neurons and robustly upregulated in reactive astrocytes (e) and microglia (f). High-magnification images show co-localization of SRR with astrocytes (g–j) and microglia (k–n) at sham, 3, and 7 dpi. Quantification of SRR expression in FACS-isolated microglia and astrocytes show that the percent of glial cells (o) and average mean fluorescent intensity per cell (p) is increased at 3 and 7 dpi as compared with sham mice. Scale bar is 100 μ m. $n = 5$ mice/group. $**p < .01$, $***p < .001$. One-way ANOVA with Tukey's multiple comparison test. Values represent mean \pm SEM. CA1, ca1 pyramidal cell layer; DG, dentate gyrus; dgc, dentate granule cell layer; pyr, pyramidal cell layer; sl, stratum lacunosum-moleculare; so, stratum oriens; sr, stratum radiatum

fluorescent intensity per cell. Astrocytes showed a trend towards an increased percentage of SRR expressing cells and mean fluorescent intensity at 3 dpi that became significant by 7 dpi. Together, these observations suggest that both microglial and astrocytic SRR contributes to pathological levels of D-serine after CCI injury.

3.2 | Changes in the cellular distribution of D-serine corresponds to SRR changes after CCI injury

D-serine is produced from L-serine by SRR enzymatic conversion. To provide direct evidence that microglia produce D-serine after CCI

injury, we examined L- and D-serine levels in hippocampal microglia by fluorescence-activated cell sorting (FACS, Figure S2) and high-performance liquid chromatography (HPLC) analysis. To reduce cellular amino acid efflux during the cell isolation, tissues were treated with amino acid transporter inhibitors throughout the isolation and FACS procedures. We observed a threefold increase in D-serine levels in isolated microglia at 3 dpi as compared with sham controls (Figure 2a), whereas isolated astrocytes showed no significant difference at 3 dpi (Figure S3a) similar to that observed for astrocytic SRR at 3 dpi (Figure 1o). By 7 dpi, SRR and D-serine levels were shown to be decreased in whole tissues from $GFAP^{creErt2};SRR^{fl/fl}$ mice as compared with $SRR^{fl/fl}$ controls (Perez et al., 2017). Examination of L-serine and

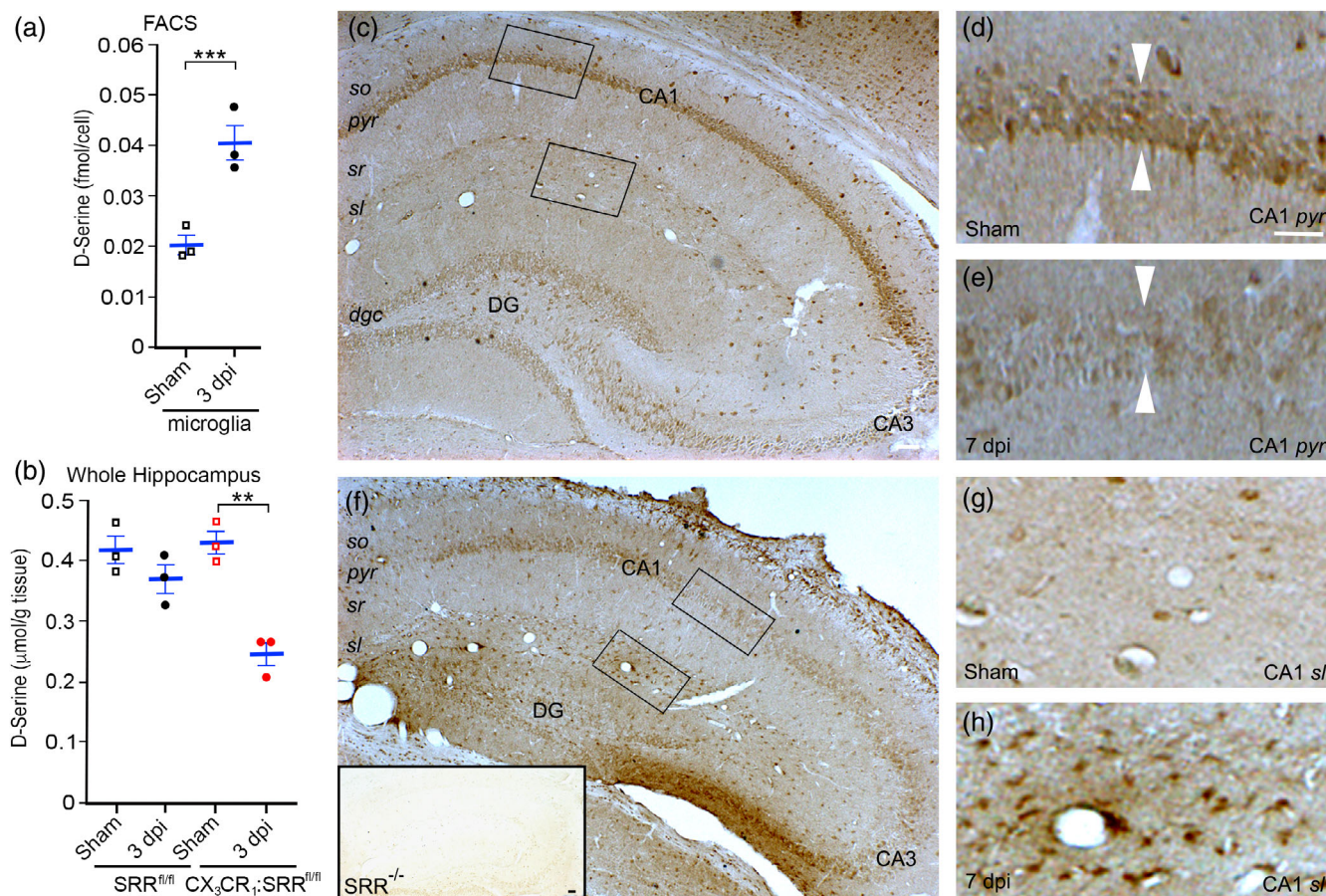


FIGURE 2 D-serine levels are increased in microglia following CCI injury. (a) HPLC analysis shows that D-serine levels are significantly increased in FACS isolated microglia at 3 dpi. (b) HPLC analysis shows that D-serine levels are not changed at 3 dpi in the whole hippocampus of $SRR^{fl/fl}$ mice as compared with sham controls, but are significantly reduced in $CX_3CR_1^{creErt2};SRR^{fl/fl}$ mice at 3 dpi. (c) D-serine is localized to hippocampal pyramidal (d, arrows) and dentate granule neurons in sham conditions, which is reduced at 3 dpi (e). (f) At 3 dpi, D-serine is reduced in *pyr* and increased in *sl* regions (h) as compared with sham controls (g). Germline knockout of SRR ($SRR^{-/-}$) shows little to no D-serine immunoreactivity (F inset). Scale bar is 100 μm . $n = 3/\text{group}$. $**p < .01$, $***p < .001$. Two-way ANOVA with Tukey's multiple comparison test. Values represent mean \pm SEM. CA1, ca1 pyramidal cell layer; CA3, ca3 pyramidal cell layer; DG, dentate gyrus; *dgc*, dentate granule cell layer; *pyr*, pyramidal cell layer; *sl*, stratum lacunosum-moleculare; *so*, stratum oriens; *sr*, stratum radiatum

L-alanine in the same cells showed no differences between microglia isolated from sham and CCI injured mice (Figure S3b,c). D-serine levels in whole hippocampal tissues from $CX_3CR_1^{creErt2};SRR^{fl/fl}$ mice were significantly reduced by twofold at 3 dpi as compared with sham controls (Figure 2b). Conversely, D-serine was not decreased in control $SRR^{fl/fl}$ mice after CCI injury. Importantly, there was also no difference in D-serine levels between sham $SRR^{fl/fl}$ and sham $CX_3CR_1^{creErt2};SRR^{fl/fl}$ mice. As previously shown (Perez et al., 2017), we typically do not observe differences in the total hippocampal D-serine level after injury, since the rise in glial D-serine is offset by the fall in neuronal D-serine. In addition, we did not observe significant changes in L-serine or L-alanine between sham and CCI injury or between $CX_3CR_1^{creErt2};SRR^{fl/fl}$ and $SRR^{fl/fl}$ mice (Figure S3d,e). Total glial D-serine levels are also dependent on cellular D-serine degradation, where enzymes, such as D-amino acid oxidase, can lead to D-serine turnover. Examination of *Daao* mRNA in the whole hippocampus showed a significant decrease at 1 dpi that returned to sham levels by

7 dpi (Figure S3f). These results demonstrate that microglial D-serine represents a significant proportion of total D-serine levels in the hippocampus only following CCI injury.

We next examined D-serine tissue expression in sham and CCI injured mice at 7 dpi using immunohistochemistry (IHC). Sham animals (Figure 2c,d,g) showed strong neuronal D-serine localization in CA1 *pyr* layer and moderate expression in the CA3 *pyr* layer and the dentate gyrus (DG). Sparse immunoreactivity was observed in the *stratum oriens* (*so*), *stratum radiatum* (*sr*), and *stratum lacunosum-moleculare* (*sl*) (Figure 2g). However, at 7 dpi (Figure 2e,f,h), there was reduced neuronal D-serine localization in the CA1 *pyr* and *dgc*, while there was robust D-serine glial immunoreactivity in *sl* and throughout the DG (Figure 2f). High-magnification images show representative comparisons of the CA1 *pyr* (arrowheads) from sham (Figure 2d) and CCI injured (Figure 2e) mice, as well as the *sl* from sham (Figure 2g) and CCI injured (Figure 2h) mice. D-serine immunoreactivity was not seen in germline $SRR^{-/-}$ null mice (Figure 2f inset). These findings support our model whereby

increased SRR expression by reactive glia following CCI injury is accompanied by a sustained increase in glial D-serine production.

3.3 | Reactive microglial and astrocytic D-serine contributes to dendritic spine damage and loss after CCI injury

We have previously shown that our CCI injury model leads to hippocampal CA1 synaptic loss in the absence of pyramidal cell death

(Perez et al., 2016). Analysis of hippocampal apical dendritic spine number and morphology provides good insight to synaptic integrity, where classic Golgi-Cox staining and analysis is still the gold standard. Here, we determined whether microglial and astrocytic SRR contributes to synaptic deficits on CA1 apical dendrites after CCI injury in $CX_3CR_1^{creErt2};SRR^{fl/fl}$ and $GFAP^{creErt2};SRR^{fl/fl}$ mice, respectively (Figure S1). In $SRR^{fl/fl}$ mice, we observed a time-dependent reduction in spine density at 3 and 7 dpi as compared with sham mice (Figure 3a). The ~25% loss in spine density by 7 dpi is similar to previous observations using transmission electron microscopy (Perez

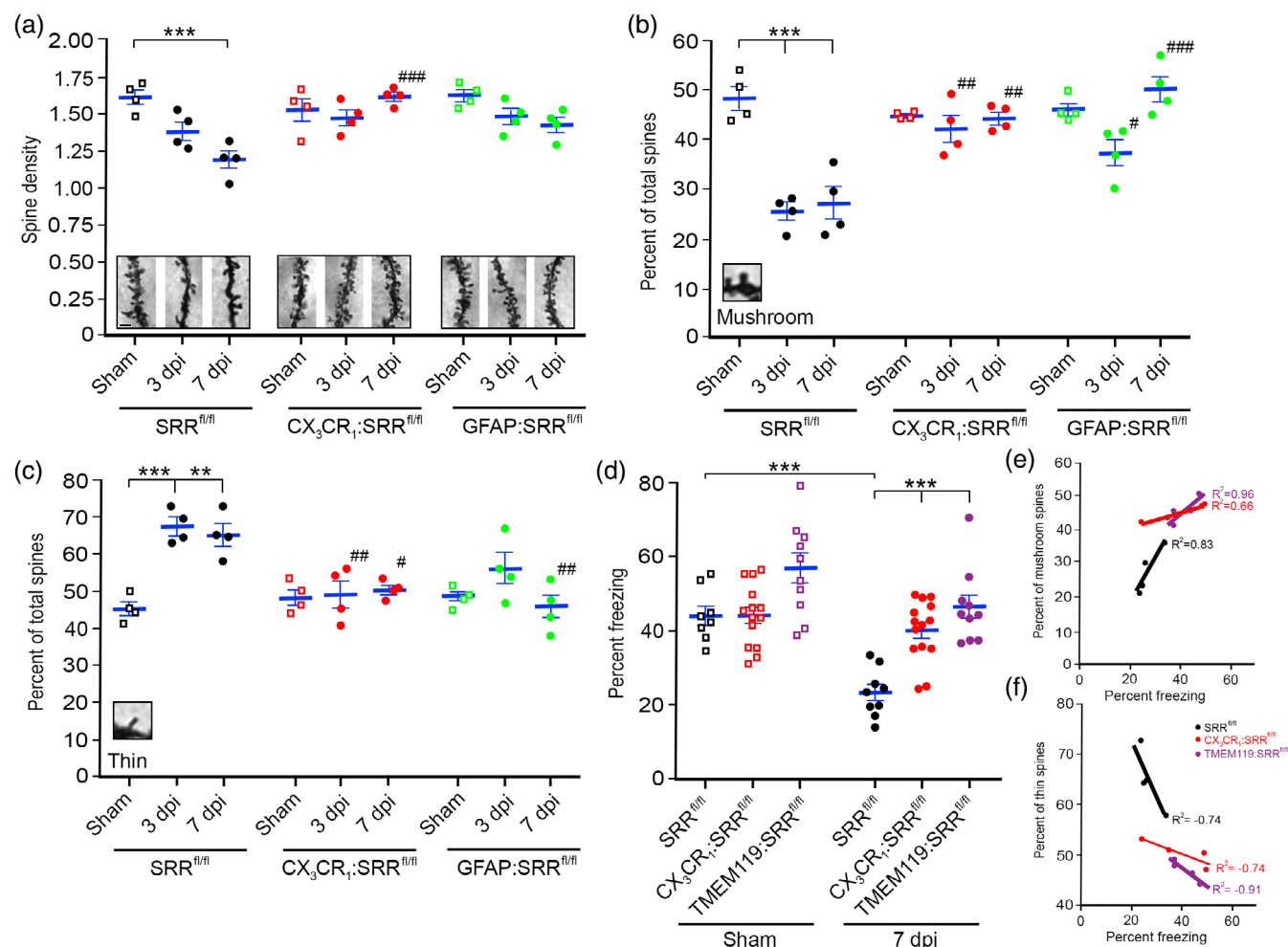


FIGURE 3 Glial SRR contributes to injury-induced dendritic spine damage as well as learning and memory deficits. (a) Spine density is significantly decreased at 3 and 7 dpi in $SRR^{fl/fl}$ mice as compared with sham controls, but not in $CX_3CR_1^{creErt2};SRR^{fl/fl}$ or $GFAP^{creErt2};SRR^{fl/fl}$ mice. Spine density is significantly increased in microglial SRR-deficient mice as compared with control $SRR^{fl/fl}$ mice at 7 dpi. Representative images for Golgi stained CA1 dendrites are shown for each group. (b) The percent of mature mushroom-shaped spines (inset image) are significantly reduced at 3 and 7 dpi in $SRR^{fl/fl}$ mice but not $CX_3CR_1^{creErt2};SRR^{fl/fl}$ or $GFAP^{creErt2};SRR^{fl/fl}$ mice. Mushroom-shaped spines are significantly increased in glial SRR-deficient mice as compared with control $SRR^{fl/fl}$ mice at 3 and 7 dpi. (c) The percent of thin spines (inset image) is increased at 3 and 7 dpi in $SRR^{fl/fl}$ mice but not $CX_3CR_1^{creErt2};SRR^{fl/fl}$ or $GFAP^{creErt2};SRR^{fl/fl}$ mice. Thin-shaped spines are significantly decreased in glial SRR-deficient mice as compared with control $SRR^{fl/fl}$ mice at 3 and/or 7 dpi. (d) Contextual fear-conditioning test shows that CCI injury leads to reduced freezing in $SRR^{fl/fl}$ mice at 7 dpi as compared with sham controls, which was not observed in $CX_3CR_1^{creErt2};SRR^{fl/fl}$ or $TMEM119^{creErt2};SRR^{fl/fl}$ mice. The percent of freezing was significantly increased in both lines of microglial SRR-deficient mice as compared with control $SRR^{fl/fl}$ mice at 7 dpi. The percent of mushroom-shaped spines correlates to percent freezing (e), while thin-shaped spines inversely correlated to percent freezing (f). $n = 4$ mice/group (a–c, e–f) and $n = 9–14$ mice/group (d). Two-way ANOVA with Tukey's multiple comparison test within genotypes or between a given timepoint. Values represent mean \pm SEM. $**p < .01$, $***p < .001$ compared with sham (within genotype); $\#p < .05$, $##p < .01$, $###p < .001$ compared with control $SRR^{fl/fl}$ mice at same postinjury timepoint

et al., 2016). Spine morphology has been classified into several different shapes (Risher et al., 2014; Rochefort & Konnerth, 2012). The two most prevalent morphologies in nonpathological conditions are mushroom-shaped, which are considered mature spines with high efficacy for synaptic transmission and plasticity, and thin-shaped, thought to represent developing or degenerating spines (Risher et al., 2014). Reduced spine density after CCI injury is due to a decrease in mushroom-shaped spines (Figure 3b) and an increase in thin spines (Figure 3c), since both morphologies are included for total spine density values. It is likely that at 3 and 7 dpi thin spines primarily represent degenerating spines, especially given the overall reduction in spine density, but newly formed spines cannot be ruled out. It is likely that the increased numbers of thin spines do not represent active synaptic units, suggesting that the cumulative functional deficits primarily represent losses in mushroom-shaped spines and synaptically inactive filopodia. This hypothesis is supported by a 50% deficit in hippocampal dependent contextual fear memory (Figure 3d), where freezing behavior positively correlates to the percentage of mushroom shaped spines (Figure 3e) and inversely correlates to the percentage of thin spines (Figure 3f). Furthermore, these findings are supported by previous studies where we observe impaired hippocampal synaptic plasticity at 7 dpi (Perez et al., 2017).

In $CX_3CR_1^{creErt2};SRR^{fl/fl}$ and $GFAP^{creErt2};SRR^{fl/fl}$ mice, we observed a significantly greater total spine density and number of mushroom-shaped spines at 3 and 7 dpi as compared with $SRR^{fl/fl}$ injured mice (Figure 3a,b). Conversely, we observed significantly fewer thin-shaped spines in both SRR-deficient glial cell types after CCI injury as compared with control $SRR^{fl/fl}$ mice (Figure 3c). In fact, spine density and the percentage of mushroom- and thin-shaped spines in $CX_3CR_1^{creErt2};SRR^{fl/fl}$ and $GFAP^{creErt2};SRR^{fl/fl}$ mice are not significantly different from sham controls. To provide additional support for the role of microglial D-serine after CCI injury, we employed a second microglial SRR deficient mouse line ($TMEM119^{CreErt2};SRR^{fl/fl}$) that employs a pan-microglial TMEM119 promoter to express cre recombinase (Kaiser & Feng, 2019). Similar to $CX_3CR_1^{creErt2};SRR^{fl/fl}$, $TMEM119^{CreErt2};SRR^{fl/fl}$ mice show a selective loss of SRR expression in Iba1+ microglia (Figure S4a–g) following CCI injury, which prevented reductions in total spine density and mushroom-shaped spines, as well as increases in thin-shaped spines (Figure S4h,i). Of note, dendritic spines were not affected in any of our sham, conditional glial SRR knockout mice. Together, these findings identify a novel role for glial D-serine in regulating dendritic spine stability after CCI injury.

3.4 | Reactive microglial and astrocytic D-serine contribute to learning and memory dysfunction

We next examined whether ablation of microglial D-serine contributes to impaired learning and memory behavior after CCI injury as previously observed for astrocytes deficient in D-serine (Perez et al., 2017). To examine learning and memory behavior, we examined freezing behavior using a fear-conditioning paradigm in $CX_3CR_1^{creErt2};SRR^{fl/fl}$, $TMEM119^{CreErt2};SRR^{fl/fl}$ and $SRR^{fl/fl}$ mice (Figure 3d). In this

paradigm mice were habituated to the testing environment, which was then paired with an aversive stimulus (i.e., a mild foot shock) (Maren et al., 2013). When mice are placed back in the conditioning context (24 h later), we observed ~45% freezing behavior which demonstrates that sham control $SRR^{fl/fl}$ mice learn and retain the association. We did not observe any significant difference in memory consolidation between sham $CX_3CR_1^{creErt2};SRR^{fl/fl}$ or $TMEM119^{CreErt2};SRR^{fl/fl}$ mice. At 7 dpi, control $SRR^{fl/fl}$ mice showed a significant ~50% reduction in freezing behavior when placed back in the same environment, indicating that hippocampal damage impairs fear memory consolidation. Injury-induced freezing deficits were not observed in $CX_3CR_1^{creErt2};SRR^{fl/fl}$ or $TMEM119^{CreErt2};SRR^{fl/fl}$ mice, demonstrating that D-serine produced by reactive microglia post-CCI injury impairs hippocampal-dependent memory consolidation. Comparison of mushroom-shaped or thin-shaped spine densities with freezing behavior show strong positive (Figure 3e) and negative (Figure 3f) correlations, respectively, for sham and CCI injured $SRR^{fl/fl}$, $CX_3CR_1^{creErt2};SRR^{fl/fl}$, and $TMEM119^{CreErt2};SRR^{fl/fl}$ mice. These findings suggest that hippocampal-dependent memory consolidation after CCI injury is sensitive to both microglia and astrocytic D-serine, where eliminating a single cellular source prevents memory deficits.

3.5 | D-amino acid transporters are upregulated after CCI injury in reactive microglia and astrocytes

To determine whether D-amino acid transporters regulate D-serine release from astrocytes and microglia, we examined three prominent amino acid transporters that are thought to participate in D-serine release, namely, Slc1a4 (ASCT1), Slc1a5 (ASCT2), and Slc7a10 (asc-1). qRT-PCR analysis of whole hippocampal tissues showed a significant increase in *Slc1a4* mRNA at 1, 3, and 7 dpi as compared with control sham mice (Figure 4a). *Slc7a10* mRNA was initially decreased at 1 dpi then returned to sham levels at 3 and 7 dpi (Figure 4b); however, *Slc7a10* mRNA was expressed two- to four-fold less than *Slc1a4* mRNA in the hippocampus after CCI injury (Figure 4c). Because *Slc1a5* mRNA was expressed >20-fold less than the other two transporters, we focused our studies on Slc1a4 and Slc7a10. We next determined whether increases in *Slc1a4* mRNA also reflected changes in Slc1a4 protein levels. Western blot analysis of Slc1a4 showed increased expression in the whole hippocampus at 3 and 7 dpi as compared with sham controls (Figure 4d; Figure S5).

To examine the spatial distribution and cellular specificity of the Slc1a4 transporter, we developed a *Slc1a4^{fl/fl}* mouse that contains a *LacZ* reporter gene driven by the endogenous *Slc1a4* promoter. LacZ expression was observed in a punctate pattern throughout the brain, including cortex, striatum, hippocampus, midbrain, hindbrain, and cerebellum in both sham and CCI injured tissues (Figure 4e–u). At 3 dpi, there was reduced LacZ expression in the injured cortical epicenter (large arrowhead) and surrounding tissues, while increased expression was observed in peri-lesional cortical regions (small arrowheads) as compared with sham animals (Figure 4h,i). Increased LacZ expression was also observed in the hippocampus at 3 dpi (Figure 4i,j), and in

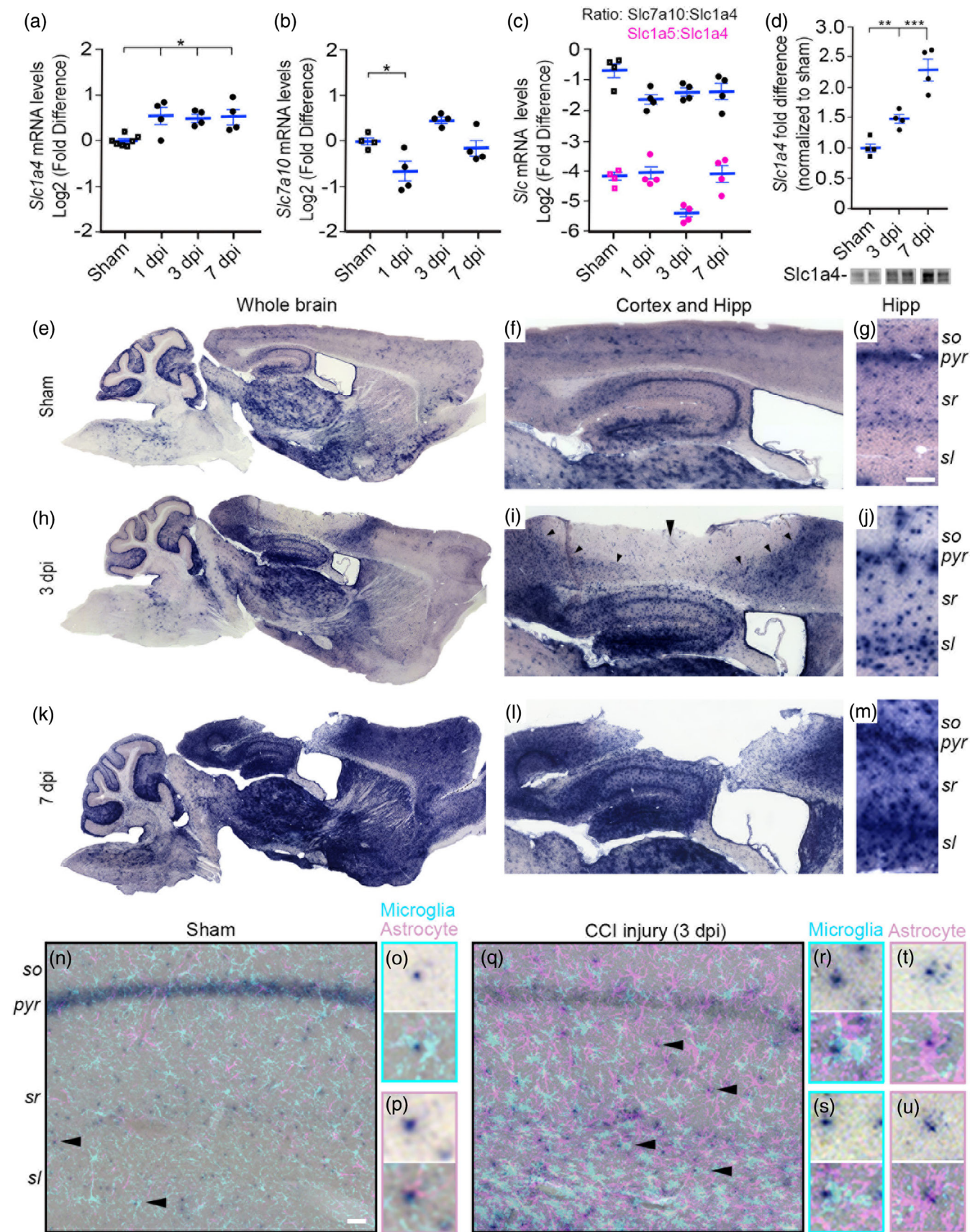


FIGURE 4 Legend on next page.



many brain regions by 7 dpi (Figure 4k–m). LacZ co-localization studies were performed in the CA1 hippocampus with α GFAP and α IBA-1 antibodies (Figure 4n–u). In sham animals and at 3 dpi, we observed that LacZ positive cells co-localized to both astrocytes and microglia, which aligns with the localization profiles of both SRR and D-serine postinjury. These findings provide evidence that reactive glia release D-serine via Slc1a4 after CCI injury.

3.6 | Pharmacologic blockade of D-amino acid transporters prevents CCI injury pathologies

To begin to assess the contribution of Slc1a4 and Slc7a10 in CCI pathology, we took advantage of a selective Slc1a4 inhibitor, L-4-chlorophenylglycine (L4), and a selective Slc7a10 inhibitor, BMS-466442 (BMS). L4 is a noncompetitive substrate inhibitor that has high selectivity and potency for Slc1a4 ($IC_{50} = 25 \mu\text{M}$) (Foster et al., 2017). BMS is a highly selective Slc7a10 inhibitor that binds via competitive occupation of an orthosteric site to prevent movement of the helices required for transport ($IC_{50} = 500 \text{ nM}$) (Brown et al., 2014; Torrecillas et al., 2019). Since Slc7a10 is an established D-serine exporter (Sason et al., 2017), application of BMS serves as a positive control for D-serine release. In our studies, inhibitors were delivered directly to the contralateral lateral ventricle using subcutaneously implanted osmotic pumps (Alzet™), and vehicle or inhibitors were infused for 7 days (harvested at 7 dpi) or 14 days (harvested at 28 dpi) (Figure 5A). The later 28 dpi paradigm was employed to determine whether blocking glial D-serine release during a critical pathological period would lead to prolonged synaptic preservation.

Based on dose escalation experiments of L4 (25, 250, 2500 μM) and BMS (0.5, 5, 50 μM), we determined that 250 μM L4 and 5 μM BMS showed the greatest protection of memory in a contextual fear conditioning paradigm after CCI injury (Figure S6a), without affecting memory in sham mice (Figure S6b). We then used these doses to show that CCI injury led to a significant, time-dependent decrease in spine density by 7 dpi in vehicle-treated mice as compared with vehicle sham controls (Figure 5b), whereas CCI injured animals treated with 250 μM L4 or 5 μM BMS showed significantly increased spine density as compared with vehicle treated CCI injury mice. In fact, spine density in CCI injured L4- or BMS-treated mice was not significantly different from sham vehicle control. Examination of synaptic

morphology showed similar improvements in L4- and BMS-treated mice, where mushroom-shaped spines were significantly increased as compared with vehicle treated CCI injured mice (Figure 5c). Conversely, CCI injury increased the number of degenerating thin spines at 7 dpi that was significantly blocked following L4 treatment. BMS showed similar trends towards reduced thin-shaped spines. Comparison of vehicle, 250 μM L4, and 5 μM BMS treated sham mice showed a slight but significant reduction in spine density and percentage of mushroom-shaped spines but no significant differences in thin spines (Figure S6c,d). This suggests that administration of 250 μM L4 or 5 μM BMS may have some additional physiological responses, where maintained inhibition of D-amino acid transporters may alter synaptic stability or remodeling. This is not surprising considering D-serine is important for maintaining appropriate dendritic spine number (Balu et al., 2012; Balu et al., 2013; Lin et al., 2016), which make the improvements observed following L4 and BMS treatment after CCI injury even more pronounced.

To determine whether 250 μM L4 treatment for 14 days followed by a “wash out” period of another 14 days (28 dpi cohort) resulted in differences in pathological outcome from 7 day treated mice, we examined the delayed effects of L4 on spine density and morphology after CCI injury. We observed similar effects of L4 treatment between the 7 and 28 dpi studies, where L4 rescued deficits in spine density and the percentage of mushroom spines and reduced the percentage of thin-shaped spines (Figure 5d,e). This suggests that the first 1–2 weeks after CCI injury is the critical period for acute synaptic damage and blocking D-serine release though Slc1a4 leads to stabilization of dendritic spines for at least 1-month postinjury.

We used a contextual fear-conditioning paradigm to determine whether L4 could prevent CCI injury-induced memory deficits. As expected, there was a significant reduction in freezing behavior in vehicle treated CCI injured mice relative to sham vehicle control mice (Figure 5f). Treatment with 250 μM L4 or 5 μM BMS prevented significant deficits in freezing behavior after CCI injury, while L4 did not affect freezing behavior in sham mice. In the 28-dpi cohort, we found a similar long-term improvement in L4 as compared with vehicle control treated CCI injured mice (Figure 5g). Together, these findings show that the synaptic pathology and cognitive impairment induced by CCI injury can be prevented by blocking the release of D-serine via both Slc1a4 and Slc7a10.

FIGURE 4 D-serine transporters are expressed in microglia and astrocytes and are altered after CCI injury. (a) Quantitative RT-PCR shows that *Slc1a4* (*ASCT1*) mRNA is upregulated at 1, 3, and 7 dpi as compared with sham controls. (b) *Slc7a10* (*asc-1*) mRNA is downregulated at 1 dpi then returns to sham levels at 3 and 7 dpi. (c) Comparison of the ratio between *Slc1a4* with *Slc7a10* or *Slc1a5* (*ASCT2*) shows ~4 and 30-fold decrease in mRNA levels, respectively. (d) Western blot analysis shows that Slc1a4 protein levels are increased at 3 and 7 dpi as compared with sham levels. LacZ reporter driven by the Slc1a4 promoter shows expression throughout the brain in sham (e–g), 3 dpi (h–j), and 7 dpi (k–m) in sagittal sections. Cortical tissues show reduced LacZ expression in the injury epicenter (large arrow) at 3 dpi (i), while peri-lesional regions (small arrows) have increased expression (including the hippocampus). (l) Increased expression is observed throughout the brain at 7 dpi. (g, j, m) high-magnification image of CA1 hippocampus. (n–u) Co-labeling of LacZ with immunofluorescent markers for microglia (α IBA1, cyan) and astrocytes (α GFAP, magenta) show co-localization of LacZ with microglia and astrocytes in sham (o, p) and at 3 dpi (r–u). Scale bar is 100 μm (g) and 50 μm (n). n = 4 mice/group (a–d) and n = 5 mice/group (e–m). One-way ANOVA with Tukey's multiple comparison test. Values represent mean \pm SEM. * $p < .05$, ** $p < .01$, *** $p < .001$. pyr, pyramidal cell layer; sl, stratum lacunosum-moleculare; so, stratum oriens; sr, stratum radiatum

3.7 | Ablation of *Slc1a4* in microglia or astrocytes protects synaptic density and memory after CCI injury

We next examined whether *Slc1a4* ablation in microglia ($CX_3CR_1^{creErt2};Slc1a4^{fl/fl}$) or astrocytes ($GFAP^{creErt2};Slc1a4^{fl/fl}$) (Figure S7a,b) would prevent CCI injury from perturbing hippocampal dendritic spine integrity and memory. CCI injury in control $Slc1a4^{fl/fl}$

mice significantly decreased both spine density (Figure 6a) and the percentage of mushroom-shaped spines (Figure 6b) but increased the percentage of thin-shaped spines (Figure 6c) compared with sham controls. These effects were reversed in $CX_3CR_1^{creErt2};Slc1a4^{fl/fl}$ and $GFAP^{creErt2};Slc1a4^{fl/fl}$ CCI injured mice. Using a fear-conditioning paradigm, CCI injury-induced memory deficits were observed in control $Slc1a4^{fl/fl}$ mice, but not in $CX_3CR_1^{creErt2};Slc1a4^{fl/fl}$ and

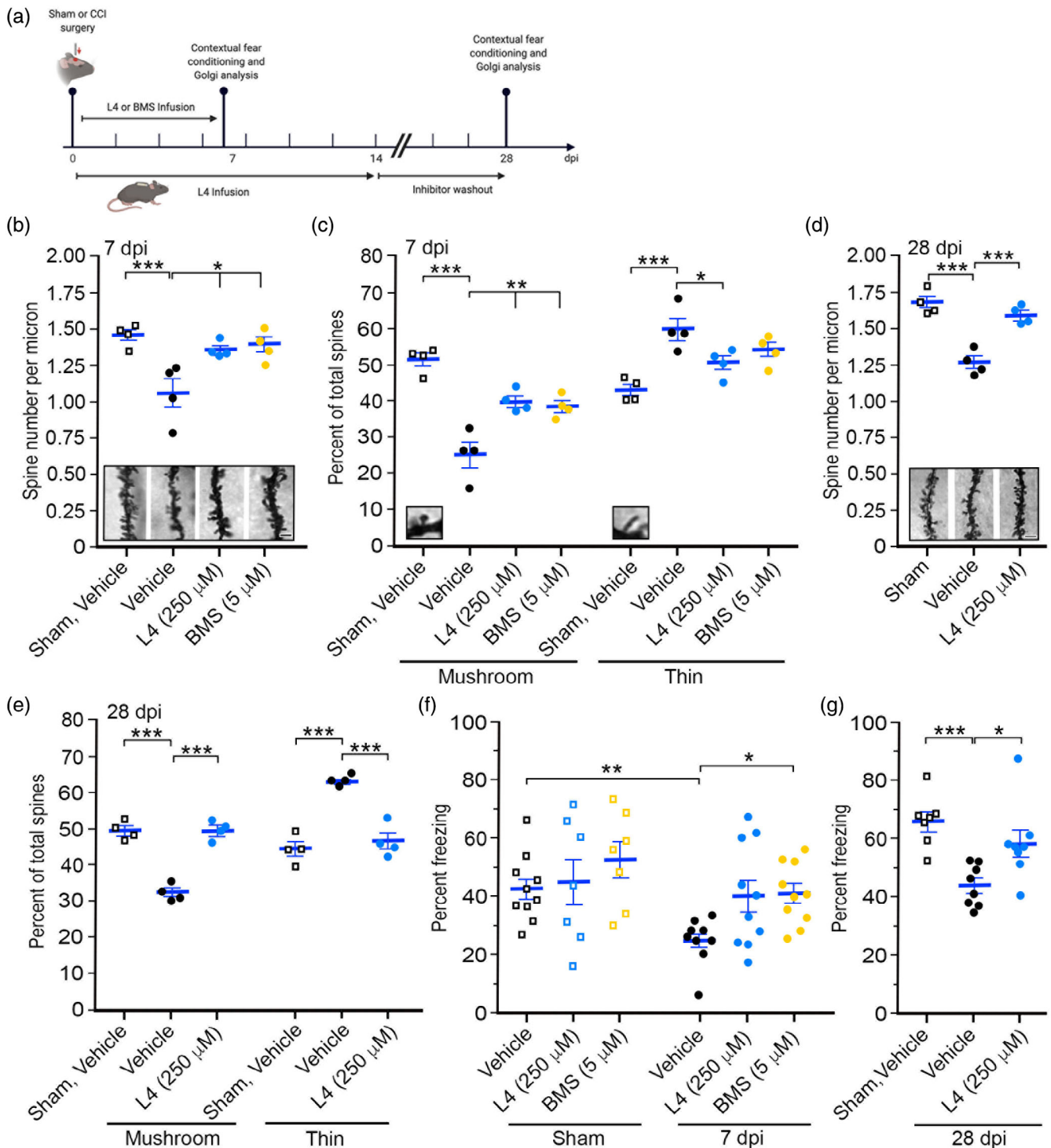


FIGURE 5 Legend on next page.

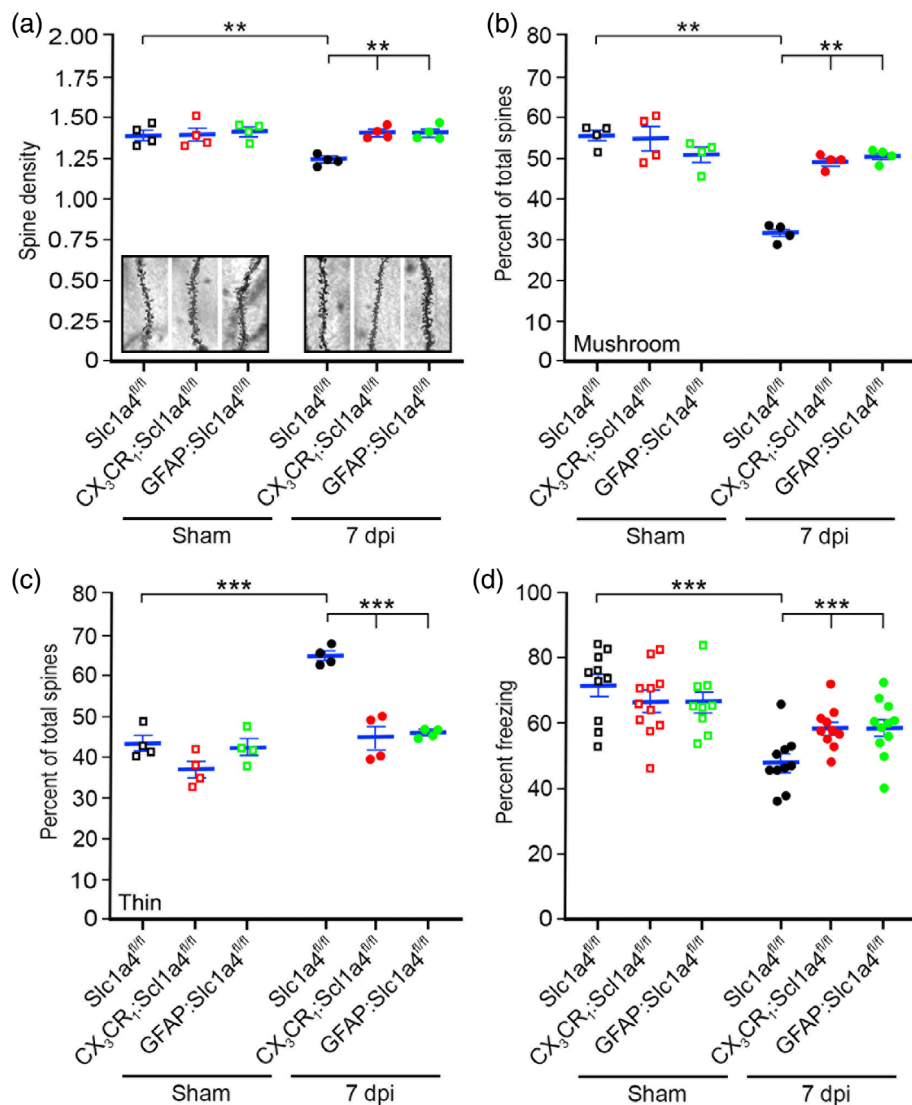


FIGURE 6 Genetic deletion of microglial and astrocyte Slc1a4 protects synapses from damage after CCI injury. (a) Spine density is significantly decreased at 7 dpi in *Slc1a4^{fl/fl}* mice as compared with sham controls, but not in *CX₃CR₁^{creErt2}:Slc1a4^{fl/fl}* or *GFAP^{creErt2}:Slc1a4^{fl/fl}* mice. Representative images for Golgi stained CA1 dendrites are shown for each group. (b) The percent of mature mushroom-shaped spines is significantly reduced at 7 dpi in *Slc1a4^{fl/fl}* mice as compared with sham controls, but not in *CX₃CR₁^{creErt2}:Slc1a4^{fl/fl}* or *GFAP^{creErt2}:Slc1a4^{fl/fl}* mice. (c) The percent of thin spines are increased at 7 dpi in *Slc1a4^{fl/fl}* mice as compared with sham controls, but not in *CX₃CR₁^{creErt2}:Slc1a4^{fl/fl}* or *GFAP^{creErt2}:Slc1a4^{fl/fl}* mice. (d) Contextual fear-conditioning test shows that CCI injury leads to reduced freezing in *Slc1a4^{fl/fl}* mice as compared with sham controls at 7 dpi, but not in *CX₃CR₁^{creErt2}:Slc1a4^{fl/fl}* or *GFAP^{creErt2}:Slc1a4^{fl/fl}* mice. $n = 4$ mice/group (a–c) and $n = 9$ –11 mice/group (d). Two-way ANOVA with Tukey's multiple comparison test within genotypes or between a given timepoint. Values represent mean \pm SEM. ** $p < .01$, *** $p < .001$ compared with sham

GFAP^{creErt2}:Slc1a4^{fl/fl} mice (Figure 6d). These genetic findings together with pharmacological L4 administration data clearly demonstrate that Slc1a4-mediated transport of reactive glial D-serine

contributes to the synaptic pathology and memory impairments caused by TBI but does not contribute to the maintenance of dendritic spine integrity or fear memory under physiological conditions.

FIGURE 5 Pharmacological inhibitors of D-amino acid transporters reduce synaptic damage after CCI injury. (a) Schematic experimental timeline. (b) Spine density is significantly decreased at 7 dpi in vehicle treated C57BL/6 wild type mice as compared with sham vehicle controls. Spine density is significantly increased when 250 μ M L-4-Chlorophenylglycine (L4) or 5 μ M BMS-466442 (BMS) is infused into the contralateral ventricle for the 7-day recovery period. Representative images for Golgi stained CA1 dendrites are shown for each group. (c) The percent of mature mushroom-shaped spines (inset image) are significantly reduced at 7 dpi, but not in L4 or BMS treated mice. L4 and BMS led to a significant increase in mushroom-shaped spines over this 7-day period. Conversely, thin spines (inset image) are increased at 7 dpi but not in L4 or BMS treated mice. L4 led to a significant decrease in thin-shaped spines over this 7-day period. (d) Infusion of L4 for 14-days followed by examination of spine density at 28 dpi showed that decreases observed in vehicle injured mice are reversed at 28 dpi. Representative images for Golgi stained CA1 dendrites are shown for each group. (e) The percent of mature mushroom-shaped spines remains significantly reduced at 28 dpi, but not in L4 treated mice, where L4 treatment led to a significant increase in mushroom-shaped spines. Conversely, thin spines remain increased at 28 dpi but not in L4 treated mice. L4 led to a significant decrease in thin-shaped spines over this 28-day period. Contextual fear-conditioning test shows that the percent freezing in vehicle treated CCI injured mice is reduced at 7 dpi (f) and 28 dpi (g) as compared with sham controls, which was not observed in L4 or BMS at 7 dpi (f) or L4 at 28 dpi (g). The percent of freezing was significantly increased in L4 and/or BMS treated mice at 7 and 28 dpi, respectively, as compared with vehicle treated mice at 7 or 28 dpi. $n = 4$ mice/group (b–e) and $n = 7$ –10 mice/group (f–g). Two-way ANOVA with Tukey's multiple comparison test within genotypes or between a given timepoint. Values represent mean \pm SEM. * $p < .05$, ** $p < .01$, *** $p < .001$

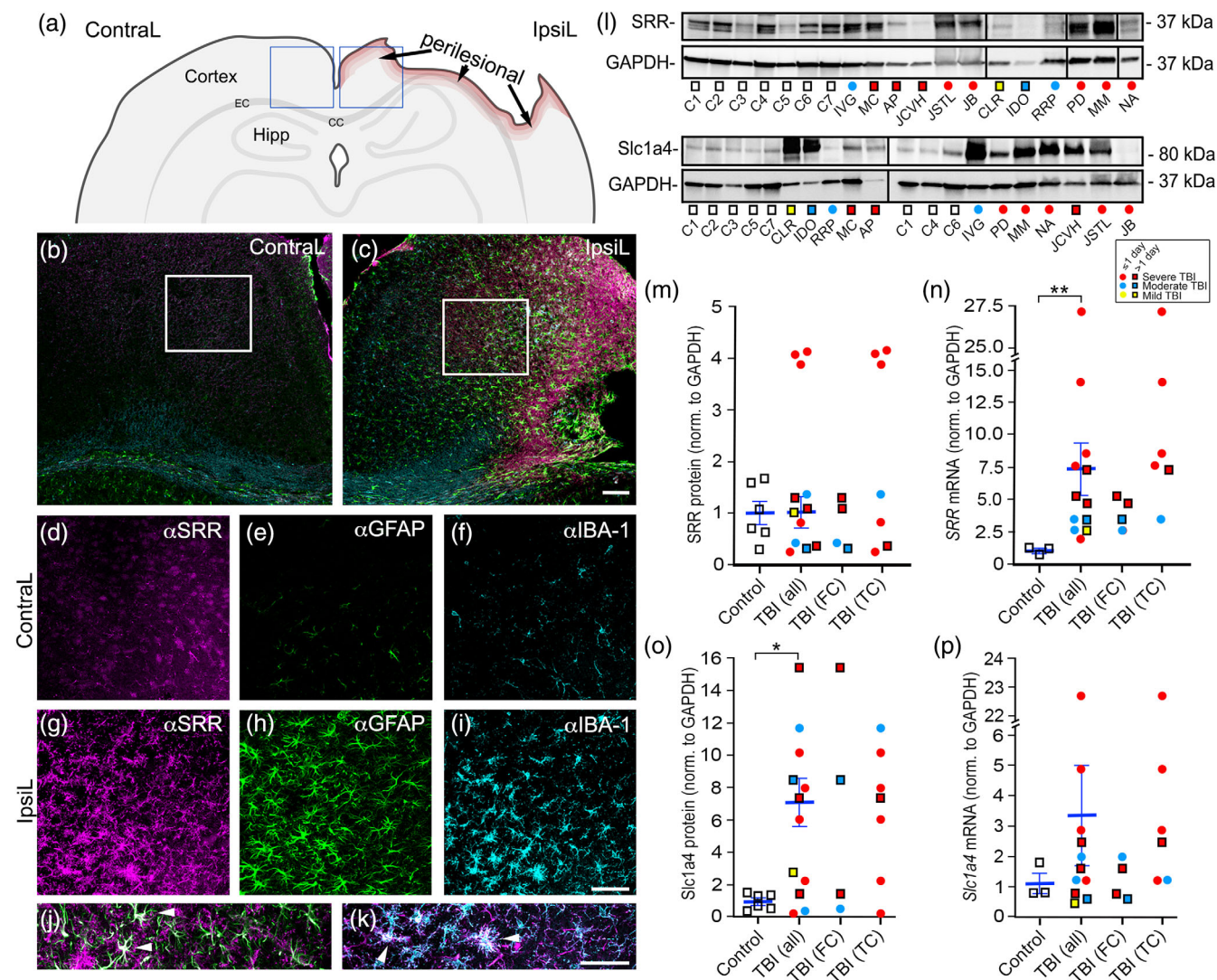


FIGURE 7 SRR is upregulated in cortical tissues in CCI injured mice and human TBI patients. (a) Schematic of perilesional tissue used for ipsilateral (IpsiL) and contralateral (ContraL) tissue analysis (Boxes). Confocal analysis of ContraL medial cortex shows little α SRR, α GFAP, or α IBA-1 immunoreactivity (b), while IpsiL medial cortex shows increased expression (c). High-magnification confocal image of ContraL α SRR (d), α GFAP (e), α IBA-1 (f), and IpsiL α SRR (g), α GFAP (h), and α IBA-1 (i). Co-labeled image of α SRR and α GFAP (j) or α SRR and α IBA-1 (k) demonstrate that SRR is expressed in reactive astrocytes and microglia, respectively. (l) Western blot analysis of α SRR and α Slc1a4 in human resected TBI tissues from seven controls (C1–C7) and 12 TBI patients (see Table 1). The key shows that TBI patient samples were segregated into their levels of severity based on the Glasgow Coma Scale, where scores ranging from 13–15 represented a mild TBI (yellow symbol), 9–12 represented a moderate TBI (blue symbol), and 3–8 represented a severe TBI (red symbol). In addition, patients were classified into two categories based on the time of injury to the time of surgical resection: either less than or equal to 1 day (circle) or greater than 1 day (square). Histograms showing distribution of SRR protein (m), SRR mRNA (n), Slc1a4 protein (o), and Slc1a4 mRNA (p) show upregulated levels of SRR and/or Slc1a4 in most patients. Values represent mean \pm SEM. * $p < .05$, ** $p < .01$ compared with human control samples

3.8 | Expression of SRR and Slc1a4 are upregulated in peri-lesional tissues from injured mouse and human brain

To determine whether changes in SRR and Slc1a4 expression are also present in peri-lesional cortical tissues, we examined the damaged murine cortex after CCI injury (3 dpi) and damaged human cortex after TBI. In the contralateral (ContraL) medial cortex of our murine model (Figure 7a), we observed minimal astrogliosis (α GFAP; Figure 7b,e), microgliosis (α IBA-1; Figure 7b,f), or SRR localization in reactive glia

(Figure 7b,d). However, in the ipsilateral (IpsiL) medial cortex (Figure 7c,g–i), there was extensive reactive gliosis that associated with increased SRR, GFAP, and Iba-1 expression. High-magnification confocal images show co-localization of SRR (Figure 7g) with reactive astrocytes (Figure 7h,j) and microglia (Figure 7i,k), where arrowheads depict representative co-labeled cells (Figure 7j,k). These findings were further supported in a mild (2 m/s) CCI injury model, where gliosis, but little to no tissue loss, is observed (Assis-Nascimento et al., 2016). Flow cytometric analysis of isolated astrocytes or microglia from the mild CCI injured cortex showed an increase in the



mean SRR fluorescent intensity at 7 dpi (Figure S7c). We also observed widespread increases in LacZ expression in the *Slc1a4^{LacZ}* reporter mice at 3 and 7 dpi (Figure 4i,l), further supporting the concept that global glial reactivity may lead to D-serine-mediated synaptic damage in cortical tissues.

We next examined SRR and Slc1a4 protein and mRNA levels in peri-lesional tissues resected from 12 TBI patients and human cortical control specimens (Figure 7l-p; Figure S8; Table 1). It was important to measure both protein and mRNA levels since protein stability may be compromised in patients that undergo surgery hours to day(s) post-TBI. Thus, we evaluated SRR, Slc1a4, and GAPDH using gel electrophoresis and qRT-PCR. Control lysates include a whole brain (C1) specimen to normalize across gels and six cortical specimens (C2-C7), while three separate mRNA control specimens represent mRNAs from cortical specific regions of combined (4-14) individuals that suffered cardiac arrest (Table 1). TBI patients were segregated into levels of severity based on the Glasgow Coma Scale, where scores ranging from 13-15 represent a mild TBI (yellow symbol), 9-12 represent a moderate TBI (blue symbol), and 3-8 represent a severe TBI (red symbol). In addition, patients were classified into two categories based on the time of injury to the time of surgical resection: either less than or equal to 1 day (circle) or greater than 1 day (square). For TBI samples, mRNA and protein lysates were extracted from the same patients (Table 1).

Analysis of SRR protein levels showed a distribution ranging from ~0.3 to 4.1-fold increase (mean of 1.6 ± 0.4) as compared with the control mean (Figure 7m), and mRNA ranged from ~2 to 27-fold increase (mean of 4.5 ± 1.1) (Figure 7n). In our SRR Western blot, we did observe a distributional difference where three of five severe (<1 day) TBI patients showed the greatest increases (Figure 7m), while SRR mRNA levels were significantly increased in all TBI samples tested (Figure 7n). This variance could be attributed to transcriptional versus translational differences at the time of tissue harvesting, but also could be due to increased degeneration of the cytosolic SRR protein postinjury. Analysis of the D-serine transporter Slc1a4 showed protein distribution ranged from ~0.2 to 15-fold increase (mean of 6.1 ± 1.14) as compared with the control mean (Figure 7o), and mRNA ranged from ~0.4 to 23-fold increase (mean of 3.3 ± 1.7), where 9 of 12 TBI patients showed greater than a twofold increase (Figure 7p). Together, this shows that all tested TBI patients exhibit increased protein and/or mRNA levels of SRR and/or Slc1a4 as compared with control specimens, supporting our CCI murine model and the possibility that there would be increased D-serine synthesis and/or release, respectively, following TBI.

4 | DISCUSSION

Cognitive dysfunction associated with TBI is rooted in the disruption of the brain's neuronal circuitry; however, the heterogenous nature of TBI complicates our interpretation of the underlying cause(s). In other words, circuitry dysfunction in the newly injured brain can be largely attributed to the morphological disruption in neuronal connections

because of cell death and/or synaptic damage. Although synaptic loss is a common feature of all TBIs (mild to severe), it is less clear whether pathological responses specifically target individual synapses. A pathological role for D-serine has been implicated in several neurological disorders that exhibit reactive astrogliosis, including Alzheimer's disease (Balu et al., 2019), amyotrophic lateral sclerosis (Paul & de Belleruche, 2012), and TBI (Perez et al., 2017). Here, by using various genetic and pharmacologic strategies, we directly link D-serine release from reactive glia to the pathological consequences of TBI. Importantly, we show for the first time in vivo that D-serine released by reactive microglia contributes to the synaptic damage and cognitive dysfunction caused by CCI injury. Furthermore, our data using tissue resected from TBI patients suggests that this pathological response is conserved in humans and extends beyond the injury site.

To examine the mechanisms that regulate synaptic damage, we established a CCI injury severity that causes ~25%-30% synaptic loss in the CA1 *stratum lacunosum-moleculare* independent of CA1 or CA3 pyramidal cell death (Perez et al., 2016). In this TBI model, cortical tissue is lost in the impact epicenter, while the underlying hippocampus is largely intact. This is an attractive model to study the mechanisms that regulate synaptic damage and remodeling within the complexity of brain injury, where many of the key secondary responses, such as gliosis and neuroinflammation persist. In fact, the effect of neuron-glia interactions on hippocampal synaptic function and stability after TBI are still poorly defined. Astrocytes are a key component of the tripartite synapse, and more recently microglia have been shown to participate in synaptic responses as well (Schafer et al., 2013). For example, microglia are critical for proper synaptic pruning during development (Paolicelli et al., 2011; Schafer et al., 2012; Stevens et al., 2007), where aberrant microglial activity is linked to many neurodegenerative conditions (Hong et al., 2016). Similar to astrocytes, microglia secrete many factors that modulate synaptic plasticity in the adult nervous system (Parkhurst et al., 2013; Stellwagen & Malenka, 2006; Wu et al., 2015), as well as interact with synapses in an activity-dependent manner (Tremblay et al., 2010) and regulate neuronal synchronization (Badimon et al., 2020). Following TBI, we demonstrate a novel mechanism by which reactive microglia and astrocytes directly contribute to synaptic damage and loss that is associated with cognitive dysfunction through D-serine release.

Under physiological conditions, L-serine is synthesized by astrocytes and shuttled into neurons via amino acid antiporters, where the neuronal enzyme SRR catalyzes its conversion to D-serine (Ivanov & Mothet, 2019; Wolosker et al., 1999). D-serine released by neurons is critical for normal synaptic function in the hippocampus (Balu & Coyle, 2012; Benneyworth et al., 2012; Perez et al., 2017); however, under inflammatory conditions like AD (Balu et al., 2019) and CCI (Perez et al., 2017), SRR expression is reduced in neurons and increased in reactive astrocytes, with astroglial-derived D-serine being detrimental to synaptic plasticity and memory (Perez et al., 2017). To date, the presence of SRR in microglia has been limited to cultured microglia, where inflammatory stimuli such as amyloid β and lipopolysaccharide have been shown to increase SRR expression and D-serine release (Wu et al., 2004; Wu & Barger, 2004). Our findings are the

first to identify a pathological *in vivo* role for microglial D-serine, which is uniquely synthesized in reactive microglia. In fact, we show that hippocampal TBI-induced deficits in memory consolidation and dendritic spine loss/damage as a result of prolonged D-serine release from both microglia and astrocytes, which can be prevented by abolishing D-serine synthesis (SRR ablation) or release (Slc1a4 ablation) from either cell type. This suggests that the combined increase in extracellular D-serine levels from both astrocytes and microglia is required to elicit pathological responses after injury. Therefore, either cell type is an attractive target for D-serine neuroprotective strategies in TBI patients.

Although D-serine can be released from neurons and glia through a variety of mechanisms, one of the primary methods in astrocytes is transporter-mediated release by Slc1a4 and/or Slc7a10 (Martineau et al., 2014; Rosenberg et al., 2013; Sason et al., 2017). Our studies demonstrate that Slc1a4 is a principal mechanism of D-serine release from both astrocytes and microglia, as cell-specific ablation of Slc1a4 preserves dendritic spines and fear conditioning behavior after TBI. Our findings are further supported by pharmacological administration of phenylglycine (PG) derivatives to inhibit amino acid transporters, where analogs with substitutions in the 4th position of the phenyl ring, such as L-4-phenylglycine (L4), showed the greatest and most selective activity to Slc1a4 (Foster et al., 2017). Direct ventricular administration of L4 likely targeted both microglial and astrocytic Slc1a4 and blocked the CCI-mediated damage to dendritic spines and cognitive dysfunction, which supports L4 as a potential therapeutic strategy. However, we cannot exclude the possibility that either inhibitor may crossreact with multiple transporters.

While our studies highlight the therapeutic benefits of L4 administration, they are not without limitations. For example, intraventricular administration does not model more clinically relevant delivery routes such as intraperitoneal or subcutaneous injection that may result in decreased efficacy due to low BBB permeability and half-life of L4 (Li et al., 2018). It would be of interest to test other analogs of the phenylglycine derivatives, such as L-4-fluorophenylglycine, that may have improved pharmacokinetics to L4. It should be noted that these pharmacokinetic studies were performed in young male rats and mice with intact blood-brain barriers (BBB) that do not reflect the open BBB observed in CCI injured brains. As such, future studies will need to determine pharmacodynamic and -kinetic properties of L4 and/or its derivatives in TBI. Furthermore, our current study is limited to male mice, and it remains to be explored whether the therapeutic effects of L4 after injury are dependent on biological sex. Another important question is whether blocking acute glial D-serine release will lead to long-term synaptic preservation. Our examination of synaptic preservation at 28 dpi is a first step in demonstrating that acute inhibition of glial D-serine could lead to long-term preservation of synaptic connections and cognitive function.

The specific mechanisms by which high interstitial D-serine levels cause synaptic damage after TBI remain to be elucidated. One likely possibility is that the excess D-serine released from reactive glia serves as the necessary co-agonist at extrasynaptic NMDARs that are primed for activation due to glutamate spillover, leading to sublethal

synaptic excitotoxicity (Cao et al., 2007; Castilho et al., 1999; Prins et al., 2013). In fact, NMDARs enriched in the GluN2B subunit have been shown to block pro-survival factors such as brain-derived neurotrophic factor and the phosphorylation of Erk1/2 and CREB (Bading, 2017). In the CCI injured hippocampus, Glu2NB levels are increased in the first week postinjury (Perez et al., 2016), and GluN2B has also been implicated in dendritic spine damage in models of cerebral ischemia (Pei et al., 2015), Alzheimer's disease (Shu et al., 2016), and Huntington's disease (Schmidt et al., 2020). While direct antagonism of NMDARs after TBI likely inhibits pro-survival as well as deleterious signaling (Ikonomidou & Turski, 2002), preventing the release of glial D-serine through the Slc1a4 transporter presents a novel pharmacological avenue to modulate NMDAR signaling and preserve synaptic function.

One of our more important findings is the pathological upregulation of SRR and Slc1a4 in the cortex of human TBI patients, where regions such as the frontal cortex and temporal pole are most affected. Our observations in peri-lesional tissues show that SRR or Slc1a4 were elevated in almost all of the TBI patients. This supports our observations in the CCI injured mouse cortex and suggests that SRR expression may be closely associated with diffuse gliosis and a primary component of widespread synaptic damage in human TBI patients. This concept that the pathological effects of D-serine may extend beyond the archicortex into other neocortical regions may be a characteristic of most TBI conditions, ranging from mild concussions to severe penetrating injuries. Furthermore, targeting synaptic damage in the human frontal and temporal cortices may have implications for critical behavioral centers. This includes prefrontal limbic systems that control executive functions such as working memory, attention, impulse control, and motivation as well as deficits in emotional behavior, language, and learning and memory. Each of these cognitive abnormalities has been observed in TBI patients (Dixon, 2017) and could extend beyond the initial injury epicenter, suggesting that a broad neuroprotective synaptic strategy may be important for improving patient outcome.

In conclusion, we identify a novel mechanism by which reactive astrocytes and microglia contribute to the pathophysiology of TBI by releasing D-serine. Our findings also highlight the D-serine metabolic pathway, particularly in reactive glia, as a potential therapeutic strategy to normalize synaptic pathology and memory deficits following brain injury, where ablation of D-serine synthesis or transporter-mediated release in either reactive glial cell type is sufficient to prevent TBI-induced synaptic damage and memory deficits. Finally, our results have important implications for other neurologic and neurodegenerative disorders that exhibit reactive gliosis.

Study approval: All procedures related to animal use and care were approved by the University of Miami Animal Use and Care Committee (protocol #20-061). The collection of human TBI brain tissues was conducted according to the guidelines of the Declaration of Helsinki and approved by the University of Miami Institutional Review Board (protocol #20080609).

Informed consent statement: Written informed consent was obtained for each patient involved in the study.



ACKNOWLEDGMENTS

The authors thank Maria M. Quiala-Acosta, Jose Mier, and Maria L. Cepero for technical assistance and animal husbandry, surgical procedures, as well as tissue harvesting and analysis. We would like to thank Eric Albuquerque for critical review of article. We also thank Dr. Oliver Umland's expertise for the flow cytometry and FACS studies.

CONFLICT OF INTEREST

The authors have declared that no conflict of interest exists.

AUTHOR CONTRIBUTIONS

SAT, DA, DJL, DTB, and HW all contributed to the overall study design, data analysis, and/or interpretation. MMD acquired confocal images, contributed to analysis of mild CCI injury and data interpretation. IR performed HPLC analysis and interpretation. JGV, LNC, and JRJ contributed to the acquisition of human TBI tissues. SEB and TH designed and performed immunofluorescence experiments. OOF designed, collected, and analyzed data from immunofluorescence experiments. SAT, DA, and DJL wrote the article with assistance from all the other authors. The position of co-first authors was chosen based on their respective contributions to experimental design, data acquisition and analysis, and writing of the article.

DATA AVAILABILITY STATEMENT

All data associated with this study are available in the main text or the supplementary materials.

ORCID

Stephen A. Tapanes  <https://orcid.org/0000-0002-0493-7859>

Daniel J. Liebl  <https://orcid.org/0000-0003-2680-1220>

REFERENCES

- Adams, K. L., & Gallo, V. (2018). The diversity and disparity of the glial scar. *Nature Neuroscience*, 21(1), 9–15. <https://doi.org/10.1038/s41593-017-0033-9>
- Assis-Nascimento, P., Umland, O., Cepero, M. L., & Liebl, D. J. (2016). A flow cytometric approach to analyzing mature and progenitor endothelial cells following traumatic brain injury. *Journal of Neuroscience Methods*, 263, 57–67. <https://doi.org/10.1016/j.jneumeth.2016.01.025>
- Badimon, A., Strasburger, H. J., Ayata, P., Chen, X., Nair, A., Ikegami, A., Hwang, P., Chan, A. T., Graves, S. M., Uweru, J. O., Ledderose, C., Kutlu, M. G., Wheeler, M. A., Kahan, A., Ishikawa, M., Wang, Y.-C., Loh, Y.-H. E., Jiang, J. X., Surmeier, D. J., ... Schaefer, A. (2020). Negative feedback control of neuronal activity by microglia. *Nature*, 586(7829), 417–423. <https://doi.org/10.1038/s41586-020-2777-8>
- Bading, H. (2017). Therapeutic targeting of the pathological triad of extrasynaptic NMDA receptor signaling in neurodegenerations. *The Journal of Experimental Medicine*, 214(3), 569–578. <https://doi.org/10.1084/jem.20161673>
- Balu, D. T., Basu, A. C., Corradi, J. P., Cacace, A. M., & Coyle, J. T. (2012). The NMDA receptor co-agonists, D-serine and glycine, regulate neuronal dendritic architecture in the somatosensory cortex. *Neurobiology of Disease*, 45(2), 671–682. <https://doi.org/10.1016/j.nbd.2011.10.006>
- Balu, D. T., & Coyle, J. T. (2012). Neuronal D-serine regulates dendritic architecture in the somatosensory cortex. *Neuroscience Letters*, 517(2), 77–81. <https://doi.org/10.1016/j.neulet.2012.04.020>
- Balu, D. T., Li, Y., Puhl, M. D., Benneyworth, M. A., Basu, A. C., Takagi, S., Bolshakov, V. Y., & Coyle, J. T. (2013). Multiple risk pathways for schizophrenia converge in serine racemase knockout mice, a mouse model of NMDA receptor hypofunction. *Proceedings of the National Academy of Sciences of the United States of America*, 110(26), 2400–2409. <https://doi.org/10.1073/pnas.1304308110>
- Balu, D. T., Pantazopoulos, H., Huang, C. C. Y., Muszynski, K., Harvey, T. L., Uno, Y., Rorabaugh, J. M., Galloway, C. R., Botz-Zapp, C., Berretta, S., Weinschenker, D., & Coyle, J. T. (2019). Neurotoxic astrocytes express the D-serine synthesizing enzyme, serine racemase, in Alzheimer's disease. *Neurobiology of Disease*, 130, 104511. <https://doi.org/10.1016/j.nbd.2019.104511>
- Balu, D. T., Takagi, S., Puhl, M. D., Benneyworth, M. A., & Coyle, J. T. (2014). D-serine and serine racemase are localized to neurons in the adult mouse and human forebrain. *Cellular and Molecular Neurobiology*, 34(3), 419–435. <https://doi.org/10.1007/s10571-014-0027-z>
- Benneyworth, M. A., Li, Y., Basu, A. C., Bolshakov, V. Y., & Coyle, J. T. (2012). Cell selective conditional null mutations of serine racemase demonstrate a predominate localization in cortical glutamatergic neurons. *Cellular and Molecular Neurobiology*, 32(4), 613–624. <https://doi.org/10.1007/s10571-012-9808-4>
- Billard, J. M. (2012). D-Amino acids in brain neurotransmission and synaptic plasticity. *Amino Acids*, 43(5), 1851–1860. <https://doi.org/10.1007/s00726-012-1346-3>
- Bodner, O., Radziszewsky, I., Foltyn, V. N., Touitou, A., Valenta, A. C., Rangel, I. F., Panizzutti, R., Kennedy, R. T., Billard, J. M., & Wolosker, H. (2020). D-Serine signaling and NMDAR-mediated synaptic plasticity are regulated by system A-type of glutamine/D-serine dual transporters. *The Journal of Neuroscience*, 40(34), 6489–6502. <https://doi.org/10.1523/jneurosci.0801-20.2020>
- Bradbury, E. J., & Burnside, E. R. (2019). Moving beyond the glial scar for spinal cord repair. *Nature Communications*, 10(1), 3879. <https://doi.org/10.1038/s41467-019-11707-7>
- Brown, J. M., Hunihan, L., Prack, M. M., Harden, D. G., Bronson, J., Dzierba, C. D., Gentles, R. G., Hendricson, A., Krause, R., Macor, J. E., & Westphal, R. S. (2014). In vitro characterization of a small molecule inhibitor of the alanine serine cysteine transporter –1 (SLC7A10). *Journal of Neurochemistry*, 129(2), 275–283. <https://doi.org/10.1111/jnc.12618>
- Cao, G., Xing, J., Xiao, X., Liou, A. K., Gao, Y., Yin, X. M., Clark, R. S., Graham, S. H., & Chen, J. (2007). Critical role of calpain I in mitochondrial release of apoptosis-inducing factor in ischemic neuronal injury. *The Journal of Neuroscience*, 27(35), 9278–9293. <https://doi.org/10.1523/jneurosci.2826-07.2007>
- Castilho, R. F., Ward, M. W., & Nicholls, D. G. (1999). Oxidative stress, mitochondrial function, and acute glutamate excitotoxicity in cultured cerebellar granule cells. *Journal of Neurochemistry*, 72(4), 1394–1401. <https://doi.org/10.1046/j.1471-4159.1999.721394.x>
- Dewan, M. C., Rattani, A., Gupta, S., Baticulon, R. E., Hung, Y. C., Punchak, M., Agrawal, A., Adeleye, A. O., Shrimel, M. G., Rubiano, A. M., Rosenfeld, J. V., & Park, K. B. (2018). Estimating the global incidence of traumatic brain injury. *Journal of Neurosurgery*, 1-18, 1080–1097. <https://doi.org/10.3171/2017.10.Jns17352>
- Dixon, K. J. (2017). Pathophysiology of traumatic brain injury. *Physical Medicine and Rehabilitation Clinics of North America*, 28(2), 215–225. <https://doi.org/10.1016/j.pmr.2016.12.001>
- Ehmsen, J. T., Liu, Y., Wang, Y., Paladugu, N., Johnson, A. E., Rothstein, J. D., du Lac, S., Mattson, M. P., & Hoke, A. (2016). The astrocytic transporter SLC7A10 (Asc-1) mediates glycinergic inhibition of spinal cord motor neurons. *Scientific Reports*, 6, 35592. <https://doi.org/10.1038/srep35592>
- Eroglu, C., & Barres, B. A. (2010). Regulation of synaptic connectivity by glia. *Nature*, 468(7321), 223–231. <https://doi.org/10.1038/nature09612>

- Faden, A. I., Demediuk, P., Panter, S. S., & Vink, R. (1989). The role of excitatory amino acids and NMDA receptors in traumatic brain injury. *Science*, 244(4906), 798–800. <https://doi.org/10.1126/science.2567056>
- Foster, A. C., Farnsworth, J., Lind, G. E., Li, Y.-X., Yang, J.-Y., Dang, V., Penjwini, M., Viswanath, V., Staubli, U., & Kavanaugh, M. P. (2016). D-serine is a substrate for neutral amino acid transporters ASCT1/SLC1A4 and ASCT2/SLC1A5, and is transported by both subtypes in rat hippocampal astrocyte cultures. *PLoS One*, 11(6), e0156551. <https://doi.org/10.1371/journal.pone.0156551>
- Foster, A. C., Rangel-Diaz, N., Staubli, U., Yang, J. Y., Penjwini, M., Viswanath, V., & Li, Y. X. (2017). Phenylglycine analogs are inhibitors of the neutral amino acid transporters ASCT1 and ASCT2 and enhance NMDA receptor-mediated LTP in rat visual cortex slices. *Neuropharmacology*, 126, 70–83. <https://doi.org/10.1016/j.neuropharm.2017.08.010>
- Fukasawa, Y., Segawa, H., Kim, J. Y., Chairoungdua, A., Kim, D. K., Matsuo, H., Cha, S. H., Endou, H., & Kanai, Y. (2000). Identification and characterization of a Na⁽⁺⁾-independent neutral amino acid transporter that associates with the 4F2 heavy chain and exhibits substrate selectivity for small neutral D- and L-amino acids. *The Journal of Biological Chemistry*, 275(13), 9690–9698. <https://doi.org/10.1074/jbc.275.13.9690>
- Helboe, L., Egebjerg, J., Moller, M., & Thomsen, C. (2003). Distribution and pharmacology of alanine-serine-cysteine transporter 1 (asc-1) in rodent brain. *The European Journal of Neuroscience*, 18(8), 2227–2238. <https://doi.org/10.1046/j.1460-9568.2003.02966.x>
- Hong, S., Dissing-Olesen, L., & Stevens, B. (2016). New insights on the role of microglia in synaptic pruning in health and disease. *Current Opinion in Neurobiology*, 36, 128–134. <https://doi.org/10.1016/j.conb.2015.12.004>
- Ikonomidou, C., & Turski, L. (2002). Why did NMDA receptor antagonists fail clinical trials for stroke and traumatic brain injury? *Lancet Neurology*, 1(6), 383–386. [https://doi.org/10.1016/s1474-4422\(02\)00164-3](https://doi.org/10.1016/s1474-4422(02)00164-3)
- Ivanov, A. D., & Mothet, J.-P. (2019). The plastic D-serine signaling pathway: Sliding from neurons to glia and vice-versa. *Neuroscience Letters*, 689, 21–25. <https://doi.org/10.1016/j.neulet.2018.05.039>
- Jeon, G. S., Choi, D. H., Lee, H. N., Kim, D. W., Chung, C. K., & Cho, S. S. (2009). Expression of L-serine biosynthetic enzyme 3-phosphoglycerate dehydrogenase (Phgdh) and neutral amino acid transporter ASCT1 following an excitotoxic lesion in the mouse hippocampus. *Neurochemical Research*, 34(5), 827–834. <https://doi.org/10.1007/s11064-008-9831-5>
- Kaiser, T., & Feng, G. (2019). Tmem119-EGFP and Tmem119-CreERT2 transgenic mice for labeling and manipulating microglia. *eneuro*, 6(4), ENEURO.0448-18.2019. <https://doi.org/10.1523/eneuro.0448-18.2019>
- Kaplan, E., Zubedat, S., Radziszewsky, I., Valenta, A. C., Rechnitz, O., Sason, H., Sajrawi, C., Bodner, O., Konno, K., Esaki, K., Derdikman, D., Yoshikawa, T., Watanabe, M., Kennedy, R. T., Billard, J.-M., Avital, A., & Wolosker, H. (2018). ASCT1 (Slc1a4) transporter is a physiologic regulator of brain D-serine and neurodevelopment. *Proceedings of the National Academy of Sciences of the United States of America*, 115(38), 9628–9633. <https://doi.org/10.1073/pnas.1722677115>
- Li, Y.-X., Yang, J.-Y., Alcántara, M., Abelian, G., Kulkarni, A., Staubli, U., & Foster, A. C. (2018). Inhibitors of the neutral amino acid transporters ASCT1 and ASCT2 are effective in in vivo models of schizophrenia and visual dysfunction. *The Journal of Pharmacology and Experimental Therapeutics*, 367(2), 292–301. <https://doi.org/10.1124/jpet.118.251116>
- Lin, H., Jacobi, A. A., Anderson, S. A., & Lynch, D. R. (2016). D-serine and serine racemase are associated with PSD-95 and glutamatergic synapse stability. *Frontiers in Cellular Neuroscience*, 10, 34. <https://doi.org/10.3389/fncel.2016.00034>
- Maren, S., Phan, K. L., & Liberzon, I. (2013). The contextual brain: Implications for fear conditioning, extinction and psychopathology. *Nature Reviews Neuroscience*, 14(6), 417–428. <https://doi.org/10.1038/nrn3492>
- Martineau, M., Parpura, V., & Mothet, J. P. (2014). Cell-type specific mechanisms of D-serine uptake and release in the brain. *Frontiers in Synaptic Neuroscience*, 6, 12. <https://doi.org/10.3389/fnsyn.2014.00012>
- McGinn, M. J., & Povlishock, J. T. (2016). Pathophysiology of traumatic brain injury. *Neurosurgery Clinics of North America*, 27(4), 397–407. <https://doi.org/10.1016/j.nec.2016.06.002>
- Mothet, J. P., Pollegioni, L., Ouanounou, G., Martineau, M., Fossier, P., & Baux, G. (2005). Glutamate receptor activation triggers a calcium-dependent and SNARE protein-dependent release of the gliotransmitter D-serine. *Proceedings of the National Academy of Sciences of the United States of America*, 102(15), 5606–5611. <https://doi.org/10.1073/pnas.0408483102>
- Neame, S., Safory, H., Radziszewsky, I., Touitou, A., Marchesani, F., Marchetti, M., Kellner, S., Berlin, S., Foltyn, V. N., Engelender, S., Billard, J.-M., & Wolosker, H. (2019). The NMDA receptor activation by D-serine and glycine is controlled by an astrocytic Phgdh-dependent serine shuttle. *Proceedings of the National Academy of Sciences of the United States of America*, 116(41), 20736–20742. <https://doi.org/10.1073/pnas.1909458116>
- Paolicelli, R. C., Bolasco, G., Pagani, F., Maggi, L., Scianni, M., Panzanelli, P., Giustetto, M., Ferreira, T. A., Guiducci, E., Dumas, L., Ragozzino, D., & Gross, C. T. (2011). Synaptic pruning by microglia is necessary for normal brain development. *Science*, 333(6048), 1456–1458. <https://doi.org/10.1126/science.1202529>
- Parkhurst, C. N., Yang, G., Ninan, I., Savas, J. N., Yates, J. R., 3rd, Lafaille, J. J., Hempstead, B. L., Littman, D. R., & Gan, W. B. (2013). Microglia promote learning-dependent synapse formation through brain-derived neurotrophic factor. *Cell*, 155(7), 1596–1609. <https://doi.org/10.1016/j.cell.2013.11.030>
- Paul, P., & de Belleruche, J. (2012). The role of D-amino acids in amyotrophic lateral sclerosis pathogenesis: A review. *Amino Acids*, 43(5), 1823–1831. <https://doi.org/10.1007/s00726-012-1385-9>
- Pei, L., Wang, S., Jin, H., Bi, L., Wei, N., Yan, H., Yang, X., Yao, C., Xu, M., Shu, S., Guo, Y., Yan, H., Wu, J., Li, H., Pang, P., Tian, T., Tian, Q., Zhu, L. Q., Shang, Y., & Lu, Y. (2015). A novel mechanism of spine damages in stroke via DAPK1 and tau. *Cerebral Cortex*, 25(11), 4559–4571. <https://doi.org/10.1093/cercor/bhv096>
- Perea, G., Navarrete, M., & Araque, A. (2009). Tripartite synapses: Astrocytes process and control synaptic information. *Trends in Neurosciences*, 32(8), 421–431. <https://doi.org/10.1016/j.tins.2009.05.001>
- Perez, E. J., Cepero, M. L., Perez, S. U., Coyle, J. T., Sick, T. J., & Liebl, D. J. (2016). EphB3 signaling propagates synaptic dysfunction in the traumatic injured brain. *Neurobiology of Disease*, 94, 73–84. <https://doi.org/10.1016/j.nbd.2016.06.007>
- Perez, E. J., Tapanes, S. A., Loris, Z. B., Balu, D. T., Sick, T. J., Coyle, J. T., & Liebl, D. J. (2017). Enhanced astrocytic D-serine underlies synaptic damage after traumatic brain injury. *The Journal of Clinical Investigation*, 127(8), 3114–3125. <https://doi.org/10.1172/jci92300>
- Prins, M., Greco, T., Alexander, D., & Giza, C. C. (2013). The pathophysiology of traumatic brain injury at a glance. *Disease Models & Mechanisms*, 6(6), 1307–1315. <https://doi.org/10.1242/dmm.011585>
- Risher, W. C., Ustunkaya, T., Singh Alvarado, J., & Eroglu, C. (2014). Rapid Golgi analysis method for efficient and unbiased classification of dendritic spines. *PLoS One*, 9(9), e107591. <https://doi.org/10.1371/journal.pone.0107591>
- Rocheffort, N. L., & Konnerth, A. (2012). Dendritic spines: From structure to in vivo function. *EMBO Reports*, 13(8), 699–708. <https://doi.org/10.1038/embor.2012.102>
- Rosenberg, D., Artoul, S., Segal, A. C., Kolodney, G., Radziszewsky, I., Dikopoltsev, E., Foltyn, V. N., Inoue, R., Mori, H., Billard, J. M., & Wolosker, H. (2013). Neuronal D-serine and glycine release via the Asc-1 transporter regulates NMDA receptor-dependent synaptic



- activity. *The Journal of Neuroscience*, 33(8), 3533–3544. <https://doi.org/10.1523/jneurosci.3836-12.2013>
- Safory, H., Neame, S., Shulman, Y., Zubedat, S., Radzishevsky, I., Rosenberg, D., Sason, H., Engelder, S., Avital, A., Hülsmann, S., Schiller, J., & Wolosker, H. (2015). The alanine-serine-cysteine-1 (Asc-1) transporter controls glycine levels in the brain and is required for glycinergic inhibitory transmission. *EMBO Reports*, 16(5), 590–598. <https://doi.org/10.15252/embr.201439561>
- Sakai, K., Shimizu, H., Koike, T., Furuya, S., & Watanabe, M. (2003). Neutral amino acid transporter ASCT1 is preferentially expressed in D-Ser-synthetic/storing glial cells in the mouse brain with transient expression in developing capillaries. *The Journal of Neuroscience*, 23(2), 550–560. <https://doi.org/10.1523/JNEUROSCI.23-02-00550.2003>
- Sason, H., Billard, J. M., Smith, G. P., Safory, H., Neame, S., Kaplan, E., Rosenberg, D., Zubedat, S., Foltyn, V. N., Christoffersen, C. T., Bundgaard, C., Thomsen, C., Avital, A., Christensen, K. V., & Wolosker, H. (2017). Asc-1 transporter regulation of synaptic activity via the tonic release of D-serine in the forebrain. *Cerebral Cortex*, 27(2), 1573–1587. <https://doi.org/10.1093/cercor/bhv350>
- Schafer, D. P., Lehrman, E. K., Kautzman, A. G., Koyama, R., Mardinly, A. R., Yamasaki, R., Ransohoff, R. M., Greenberg, M. E., Barres, B. A., & Stevens, B. (2012). Microglia sculpt postnatal neural circuits in an activity and complement-dependent manner. *Neuron*, 74(4), 691–705. <https://doi.org/10.1016/j.neuron.2012.03.026>
- Schafer, D. P., Lehrman, E. K., & Stevens, B. (2013). The "quad-partite" synapse: Microglia-synapse interactions in the developing and mature CNS. *Glia*, 61(1), 24–36. <https://doi.org/10.1002/glia.22389>
- Schmidt, M. E., Caron, N. S., Aly, A. E., Lemarié, F. L., Dal Cengio, L., Ko, Y., Lazić, N., Anderson, L., Nguyen, B., Raymond, L. A., & Hayden, M. R. (2020). DAPK1 promotes Extrasynaptic GluN2B phosphorylation and striatal spine instability in the YAC128 mouse model of Huntington disease. *Frontiers in Cellular Neuroscience*, 14, 348.
- Shleper, M., Kartvelishvili, E., & Wolosker, H. (2005). D-serine is the dominant endogenous coagonist for NMDA receptor neurotoxicity in organotypic hippocampal slices. *The Journal of Neuroscience*, 25(41), 9413–9417. <https://doi.org/10.1523/jneurosci.3190-05.2005>
- Shu, S., Zhu, H., Tang, N., Chen, W., Li, X., Li, H., Pei, L., Liu, D., Mu, Y., Tian, Q., Zhu, L. Q., & Lu, Y. (2016). Selective degeneration of entorhinal-CA1 synapses in Alzheimer's disease via activation of DAPK1. *The Journal of Neuroscience*, 36(42), 10843–10852. <https://doi.org/10.1523/jneurosci.2258-16.2016>
- Stellwagen, D., & Malenka, R. C. (2006). Synaptic scaling mediated by glial TNF- α . *Nature*, 440(7087), 1054–1059. <https://doi.org/10.1038/nature04671>
- Stevens, B., Allen, N. J., Vazquez, L. E., Howell, G. R., Christopherson, K. S., Nouri, N., Micheva, K. D., Mehalow, A. K., Huberman, A. D., Stafford, B., Sher, A., Litke, A. M., Lambris, J. D., Smith, S. J., John, S. W., & Barres, B. A. (2007). The classical complement cascade mediates CNS synapse elimination. *Cell*, 131(6), 1164–1178. <https://doi.org/10.1016/j.cell.2007.10.036>
- Taylor, C., Bell, J., Breiding, M., & Xu, L. (2017). Traumatic brain injury-related emergency department visits, hospitalizations, and deaths – United States, 2007 and 2013. *MMWR Surveillance Summaries*, 66(SS-9), 1–16. <https://doi.org/10.15585/mmwr.ss6609a1>
- Torreillas, I. R., Conde-Ceide, S., de Lucas, A. I., Garci, A. M. A., Trabanco, A. A., Lavreysen, H., Pardo, L., & Tresadern, G. (2019). Inhibition of the alanine-serine-cysteine-1 transporter by BMS-466442. *ACS Chemical Neuroscience*, 10(5), 2510–2517. <https://doi.org/10.1021/acscchemneuro.9b00019>
- Tremblay, M.-È., Lowery, R. L., & Majewska, A. K. (2010). Microglial interactions with synapses are modulated by visual experience. *PLoS Biology*, 8(11), e1000527. <https://doi.org/10.1371/journal.pbio.1000527>
- Wang, H., Song, G., Chuang, H., Chiu, C., Abdelmaksoud, A., Ye, Y., & Zhao, L. (2018). Portrait of glial scar in neurological diseases. *International Journal of Immunopathology and Pharmacology*, 31, 205873841880140. <https://doi.org/10.1177/2058738418801406>
- Wolosker, H. (2011). Serine racemase and the serine shuttle between neurons and astrocytes. *Biochimica et Biophysica Acta (BBA) - Proteins and Proteomics*, 1814(11), 1558–1566. <https://doi.org/10.1016/j.bbapap.2011.01.001>
- Wolosker, H. (2018). The neurobiology of D-serine signaling. In G. W. Pasternak & J. T. Coyle (Eds). *Advances in Pharmacology* (Vol. 82, pp. 325–348). Academic Press.
- Wolosker, H., Balu, D. T., & Coyle, J. T. (2016). The rise and fall of the D-serine-mediated gliotransmission hypothesis. *Trends in Neurosciences*, 39(11), 712–721. <https://doi.org/10.1016/j.tins.2016.09.007>
- Wolosker, H., Blackshaw, S., & Snyder, S. H. (1999). Serine racemase: A glial enzyme synthesizing D-serine to regulate glutamate-N-methyl-D-aspartate neurotransmission. *Proceedings of the National Academy of Sciences of the United States of America*, 96(23), 13409–13414. <https://doi.org/10.1073/pnas.96.23.13409>
- Wong, J. M., Folorunso, O. O., Barragan, E. V., Berciu, C., Harvey, T. L., Coyle, J. T., Balu, D. T., & Gray, J. A. (2020). Postsynaptic serine racemase regulates NMDA receptor function. *The Journal of Neuroscience*, 40(50), 9564–9575. <https://doi.org/10.1523/jneurosci.1525-20.2020>
- Wu, S., & Barger, S. W. (2004). Induction of serine racemase by inflammatory stimuli is dependent on AP-1. *Annals of the New York Academy of Sciences*, 1035, 133–146. <https://doi.org/10.1196/annals.1332.009>
- Wu, S. Z., Bodles, A. M., Porter, M. M., Griffin, W. S., Basile, A. S., & Barger, S. W. (2004). Induction of serine racemase expression and D-serine release from microglia by amyloid beta-peptide. *Journal of Neuroinflammation*, 1(1), 2. <https://doi.org/10.1186/1742-2094-1-2>
- Wu, Y., Dissing-Olesen, L., MacVicar, B. A., & Stevens, B. (2015). Microglia: Dynamic mediators of synapse development and plasticity. *Trends in Immunology*, 36(10), 605–613. <https://doi.org/10.1016/j.it.2015.08.008>

SUPPORTING INFORMATION

Additional supporting information may be found in the online version of the article at the publisher's website.

How to cite this article: Tapanes, S. A., Arizanovska, D., Díaz, M. M., Folorunso, O. O., Harvey, T., Brown, S. E., Radzishevsky, I., Close, L. N., Jagid, J. R., Gracioli Cordeiro, J., Wolosker, H., Balu, D. T., & Liebl, D. J. (2022). Inhibition of glial D-serine release rescues synaptic damage after brain injury. *Glia*, 70(6), 1133–1152. <https://doi.org/10.1002/glia.24161>